Master thesis – Electrical Engineering

Modelling & Evaluation of EM Effect of Metal Fills used in IC Technology

Hrishi Narayanan Kothandaraman
2022

TUDelft

NXP

Master thesis - Electrical Engineering

Modelling & Evaluation of EM Effect of Metal Fills used in IC Technology

Hrishi Narayanan Kothandaraman

November 2022

This thesis is submitted in partial fulfillment of the requirements for the degree of Master of Science in Electrical Engineering at Delft University of Technology

The work in this thesis was carried out at:

ELCA - Delft University of Technology

NXP SEMICONDUCTORS

Supervisors: Prof.dr. Marco Spirito
                    dr. Rick Janssen
Thesis Committee: Prof.dr. Alexander Yarovoy
                    Prof.dr. Marco Spirito
                    dr. Rick Janssen

Abstract

Nowadays, recent Integrated Circuit (IC) Technology demands a minimum metal fill inclusion across the entire die of each functional layer to have uniform planarity. It is challenging to numerically simulate the real structure using Electromagnetic (EM) solvers because the mesh size of an EM solver is inversely proportional to the number of vertices in the layout and the inclusion of these metal fills has a significant impact on these vertices and increases mesh size. It is important to understand the metal fills do have an impact on the RF performance of the component and the impact becomes stronger as the frequency increases due to the parasitics and hence we cannot neglect it. Therefore, a Design Flow Methodology is studied and analysed to take into account the effect of metal fills without penalty in accuracy and simulation time.

The second part of the thesis focuses on two different approaches that can be used to extract the complex parameters providing the electromagnetic response of the layers, i.e. electrical permittivity and magnetic permeability. First, we describe the Quasistatic approach to extract the epsilon parameters from the capacitance and inductance. After, describing some of the limitations of this approach we focus on the Oblique Incidence Method as reported in the literature to extract the complex epsilon tensor parameters.

The third part of the thesis looks into the Design Flow Methodology that embeds the Oblique Incidence Method into the design flow for 3D EM solvers to take into account the effect of metal fills. The 2.5D EM solver takes into account a scalar number which is less accurate and hence an insight of how the solution from the Oblique Incidence Method can used to extract a scalar number for the effective parameters and therefore be implemented in 2.5D EM tools is discussed.

The fourth part of the thesis shows the validation of the Oblique Incidence Method for the 3D EM tool for two test cases which are wave propagating structure and lumped structure namely Grounded Coplanar Waveguide (CPWG) and Stacked Transformer. Validation of the Scalar Number Approaches for the 2.5D EM Tool was done for the CPWG structure.

Finally, a brief study on the Design Based Approach is conducted with different metal fill shapes and alignment by using the Oblique Incidence Method by making use of 3D EM tool. This approach provides a better understanding of the epsilon variations for different metal fill shapes and that for less epsilon variations, an accurate scalar number value can be extracted to enable 2.5D EM simulations with improved accuracy.

Acknowledgements

Contents

List of Figures

Acronyms

1. Introduction

1.1. Technology Roadmap

1.1.1. History

Over the course of the last 50 years, Moore's Law has been the empirical principle guiding the growth of the semiconductor industry. Moore's Law is a fundamental observation and prediction that asserts that the number of transistors on a dense IC doubles every 2 years for the same price [2]. The rule is essentially an economic one because scaling devices enables more logic to be packed for less money. Because of the law's self-fulfilling prophecy character, it has significantly impacted the development of integrated circuits as well as the semiconductor industry as a whole [3].

The semiconductor industry has made significant investments to create the "Technology Nodes", which fundamentally enable faster, cheaper, and smaller circuits, starting in 1971 with the 10um technology node to some early efforts in the 5nm technology node in 2022 as shown in Figure 1.1.

1.1.2. Technology Nodes

The term technology node shown in Figure 1.2 refers to a particular semiconductor manufacturing process with a specific feature size resolution which requires specific design guidelines to be followed to achieve the required process yield and repeatability. In general, a smaller technology node translates into reduced feature sizes of the process, which results in a faster, more power efficient transistor owing to the reduced value of the parasitic elements (i.e. R and C) [4].

The term started to be a talking point around 1990's when higher switching frequency was driving the development of microprocessors and higher capacity was driving the development of Dynamic Random Access Memory (DRAM). DRAM started to be the main driver of "Technological Scaling" because increasing densities allowed for greater capacity. Up until the early 2000s, this remained the situation. The semiconductor industry receives direction and support from The International Technology Roadmap For Semiconductors (ITRS), on a variety of technology nodes [5].
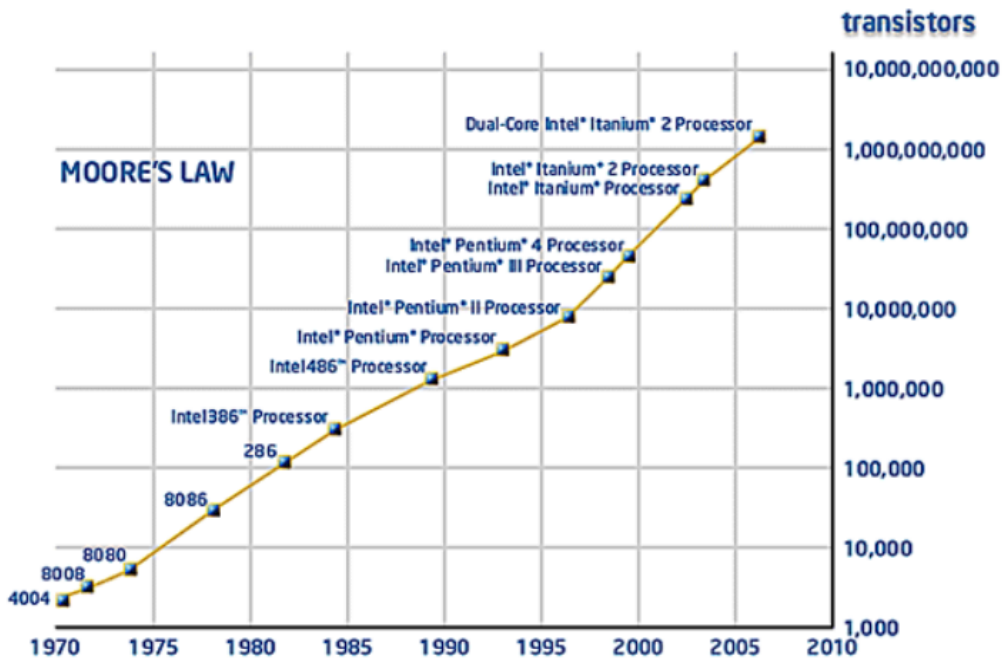
Figure 1.1.: Moore's Law
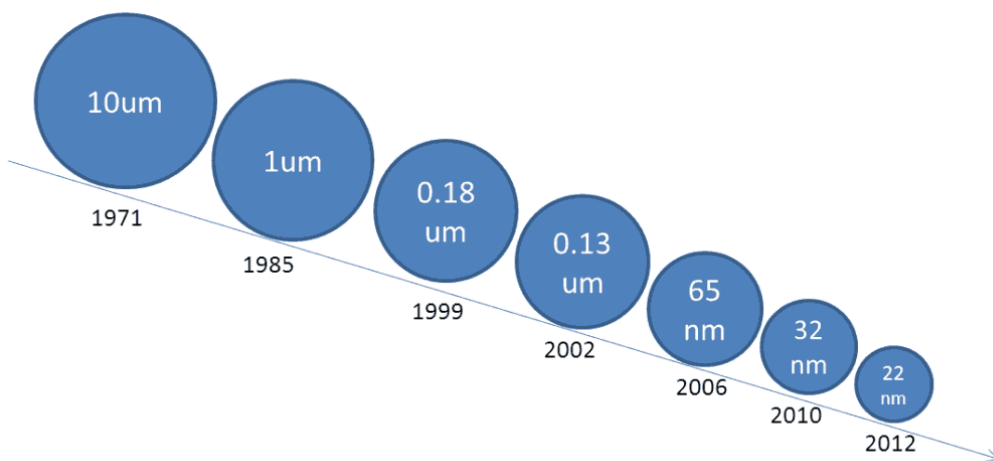
Figure 1.2.: Technology Nodes

(a)

(b)
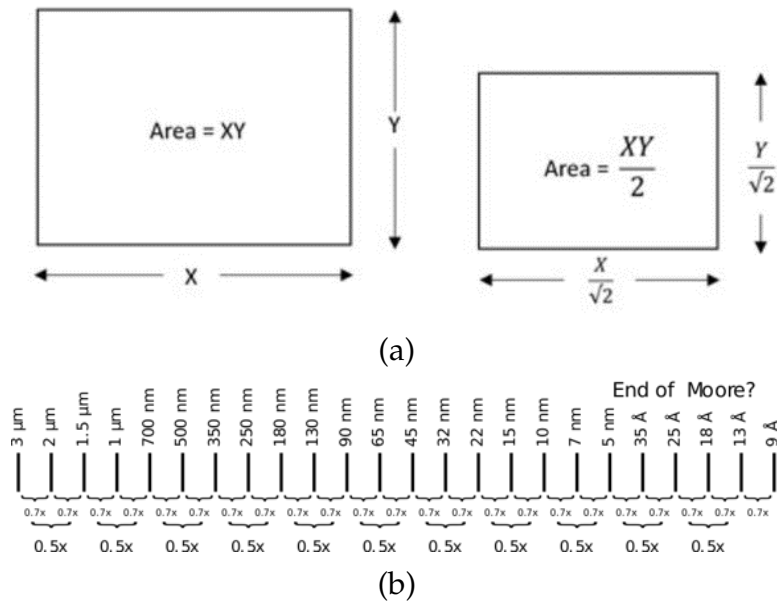
Figure 1.3.: (a) Percentage reduction in area (b) Scaling Trends

1.1.3. Technology Scaling And Its Impact

The evolution of fabrication process provides improvements, known as "Scaling" trends, which is independent from the possible circuit/architectural innovation. Thirty percent reduction in the dimensions reduces the area by fifty percent thus inducing a scaling factor of 0.7x as shown in Figure 1.3[2]. This scaling factor of 0.7x provides a guideline to interpret the various process nodes from 180nm to 180*0.7=130nm to 130*0.7=90nm to 90*0.7=65nm to 45nm, 32nm, 22nm, 16nm and so on.

Reduction in the size of the devices reduces effective capacitance which in turn reduces device delay by thirty percent making devices run faster and also enhances the performance in terms of power consumption [6].

With the clear performance and area usage advantages of the scaling approach seen on one side, there are also some strict requirements from the foundries which are a direct consequence of this approach. First, in order to take into account these small devices, all the disturbances on the wafer (i.e. larger structures) would be detrimental on the overall performance [6]. Hence, there has to be a strong consistency across the wafer that has to be enforced by manufacturers. In order to do this, the manufacturers set specific type of space occupancy rules[7]. The implication of these strict set of rules, when applied to metal back-end layers, the accurate inclusion of their effect on the design performance will be the focus in this thesis work.
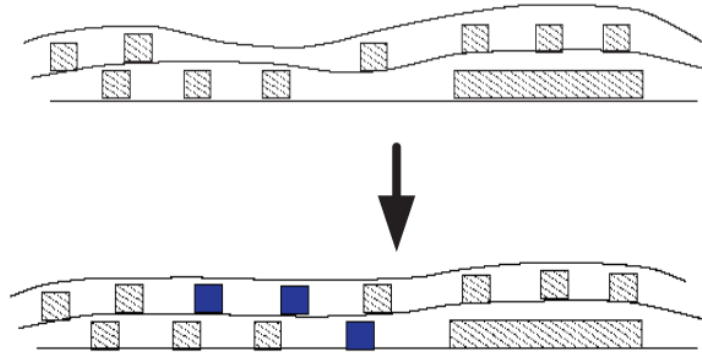
Figure 1.4.: Uniform Planarity

1.2. Metal Fill Density and its Rules

1.2.1. The Use Of Metal Fill Density

The IC design flow includes the metal fills which is a requirement to achieve reliable and repeatable manufacturing. Metal fill structures have been initially applied to increase layer planarity over the entire wafer. It entails structural forms or polygon shapes, which are electrically neutral (i.e. floating) in the design. Filling up the open areas of a design with non-functional metal forms results in a more uniform distribution of metal across the die shown in Figure 1.4 [8]. Because of homogeneity of the metal density, thickness fluctuations that happen during the manufacturing processes are reduced.

Metal fills were frequently added and known as floating or dummy fills in the earlier technology nodes. For smaller geometrical structures, design rules are far more complex necessitating earlier metal fill handling in the implementation phase. It can now control manufacturing processes like electrochemical deposition, etching, lithography in addition to enhancing planarity [9].

1.2.2. Design Rule Checks and Metal Fill Density Rules

Design Rule Checks (DRC) are nothing more than physical examinations of metal width, pitch, and spacing requirements for various layers, which vary depending on technology nodes. Due to the complexity of the advanced nodes (130nm,65nm,28nm), the number of rules increases as shown in Figure 1.5. For manufacturability, a design's layout must adhere to a set of specified technology norms provided by the foundry. An automated program will review each polygon (shape) in the design against these design principles when the layout and physical connections are finished and it will flag any violations [10]. The DRC of the design needs to be cleaned before design submission to the foundry else will not proceed to fabrication[11].
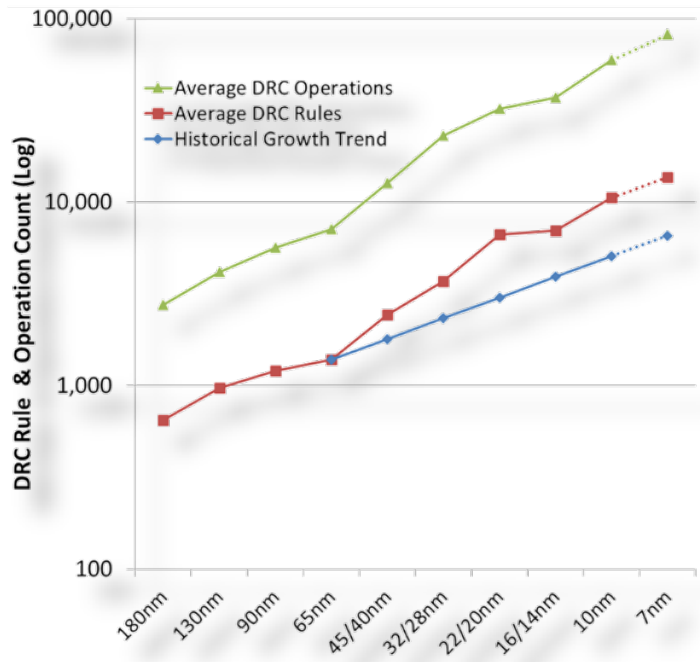
Figure 1.5.: Design Rules

In the earlier technology nodes, metal fills density rules were only defined by DRC. Utilization of metal density is limited by a minimum and maximum constraint. Limits are typically 30 percent $\leq$ metal density $\leq$ 80 percent. The criteria used to assess a quality fill result at today's advanced nodes is no longer limited to the minimum and maximum density levels specified by DRC. The added rules [12]: i) The perimeter of the fill shapes, ii) The density gradient iii) Difference in density between adjacent layout sections, are all now included during the metal fill density checks.

Furthermore, as mentioned earlier, manufacturing teams are employing metal fills to address problems with stress, etch, and rapid thermal annealing. Clearly, all of these additional density specifications must be reached without having an influence on design performance. Figure 1.6 shows how metal fills are placed under structures.

1.2.3. High Frequency Application

High frequency systems are complex to design and optimize and their application space is continually spreading in various commercial markets, such as telecom, automotive, industrial, etc. Accurate modeling and optimization of high-frequency systems is a key requirement to reach commercial viability and the short development cycles required by these markets. Hence, in order to capture the intricate effects (e.g. requiring good accuracy and prediction not only with the resistance and capacitance of the layers that is used but also the inductance), EM solvers were
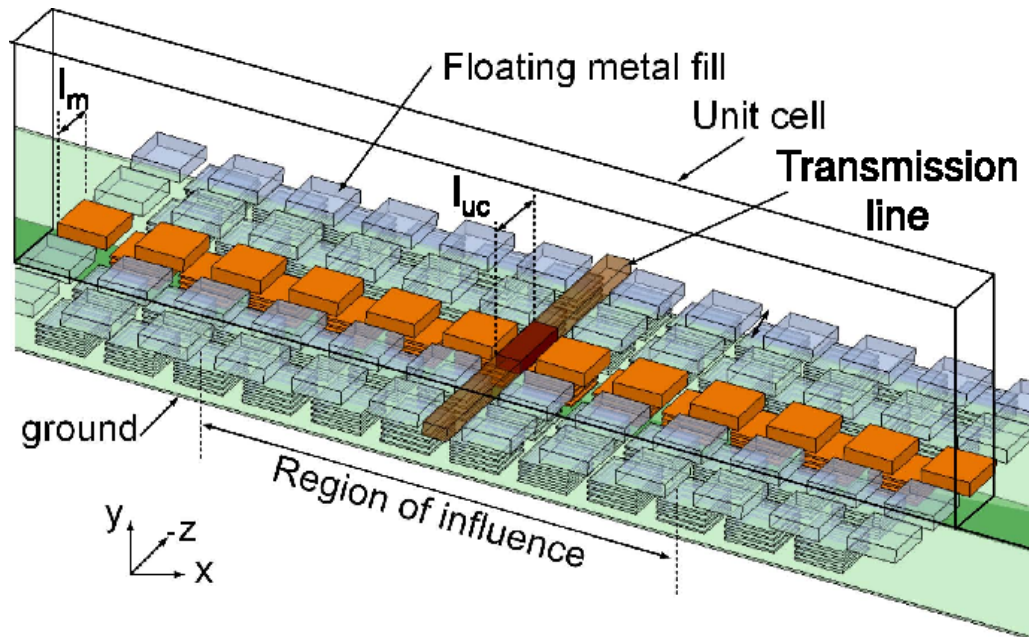
Figure 1.6.: Metal fill structures [1]

introduced. EM simulation is becoming an essential step in the design flow of integrated circuits aiming at high frequency applications. Large sections up to the entire system can be accurately modeled with modern commercial EM tools [13].

1.3. Challenges Faced by EM Simulators and Metal Fills Research Challenges

1.3.1. EM Simulation Challenges

As mentioned in the previous subsection, higher frequencies require EM solvers in order to take into account complicated effects. We need to brush up on a few concepts before we look at the challenges faced by the EM solver.

i) Solution of Maxwell Equation and Boundary Condition - EM solvers are programs that basically solve Maxwell's equation directly as shown below. The solutions of Maxwell equations are electric or magnetic fields. The intricate effects require the use of appropriate form of Maxwell's equations for high frequency systems where the structure geometries are complicated. The first form of Maxwell's equation makes use of differential form shown below and for this, the meshing takes place over the entire area where electromagnetic fields reside. FEM and FDTD uses this form of Maxwell's equation. The second form of Maxwell's equation makes use of integral and for this, the meshing takes place only for the sources of electromagnetic field. These sources can be physical quantities like the surface charge density for capacitance problem. MoM uses this form of Maxwell's equation. To resolve the fields for a domain under consideration, one has to specify the characteristics of this

field at the boundaries that separate two different domains with different physical properties. The boundary condition of the cell is considered as the modus operandi of the solver [14]. It is essential to let the EM tool understand how the behavior of the field is. Hence, the boundary conditions enable the solutions to be faster and more accurate.

$$\nabla \times H = \frac{\partial \mathcal{D}}{\partial t} + J_f \qquad \text{(Ampere's Law)}$$

$$\nabla \times E = -\frac{\partial \mathcal{B}}{\partial t} \qquad \text{(Faraday's Law)} \qquad (1.1)$$

$$\nabla \cdot \mathcal{B} = 0 \qquad \text{(Gauss's Law for magnetism)}$$

$$\nabla \cdot \mathcal{D} = 0 \qquad \text{(Gauss's Law)}$$

ii) Meshing - Meshing is defined as a process where a continuous structure is broken down into many shapes to accurately define the physical shape of the structure. Mesh generation plays a significant role in EM simulation process because meshing influences the accuracy of the solution, speed of the simulation and convergence. The solvers cannot directly simulate on the model's actual shape as the Maxwell equation cannot be applied to a random shape and hence mesh elements allow the Maxwell equations to be solved on predictable shape and mathematically defined volumes. The most common mesh element shapes are Quadrilateral and Triangle for 2D structures, Hexahedral and Tetrahedral for 3D structures which is basically a collection of vertices, edges and faces [15]. Mesh size depends on the number of vertices, edges and face. Higher the vertices, mesh size increases and hence simulation time increases. Mesh density determines the accuracy of the result and therefore the simulation time. The right balance has to be found in order to satisfy both the requirements.

The challenges faced by the EM solvers are as follows:

i) Figure 1.7 shows that the technological layer stack is very complex with small separation among layers with different thickness.

ii) Modern IC technology demands a minimum metal coverage across the entire die for each functional layer. In order to satisfy this need, several dummy metal fills are automatically added to every layer by scripts. Since the mesh size of an EM solver is linked to the number of vertices in the layout, the inclusion of these dummy metal fills has tremendous impact on these vertices and increases mesh size making it difficult to simulate the real structure numerically using EM solvers as shown in Figure 1.8. For example, if we consider an area 100um2 with the metal fill dimension of 0.5 micron (i.e.length and width) and spacing of 0.75 micron between metal fills. This would result in close to 10000 metal fills in this area. So, now we can imagine how difficult it would be to mesh 10000 metal fills and hence simulating these small structures can be really difficult. Figure 1.9 illustrates the DRC requirements that
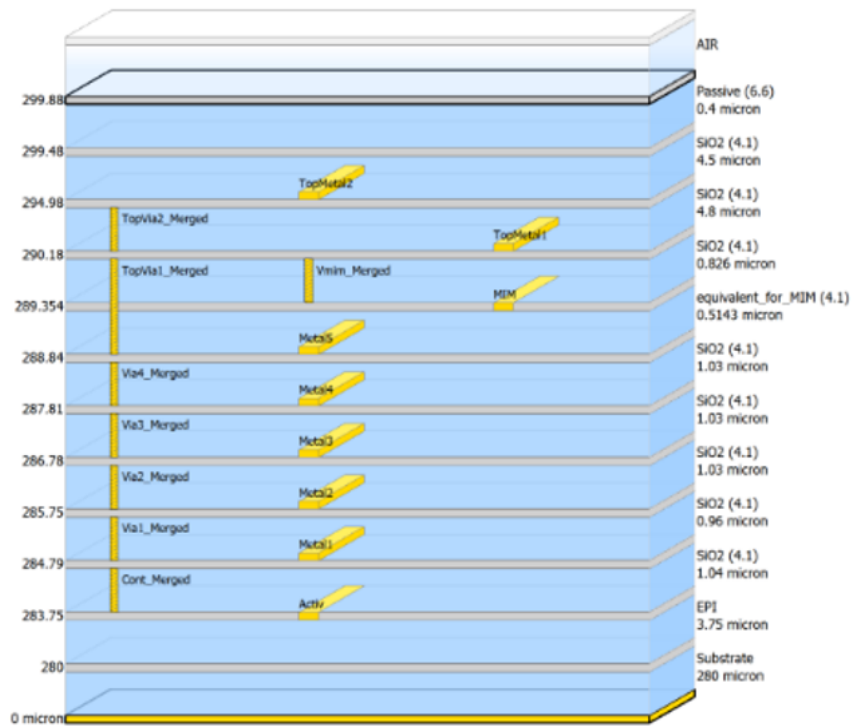
Figure 1.7.: Layer Stack
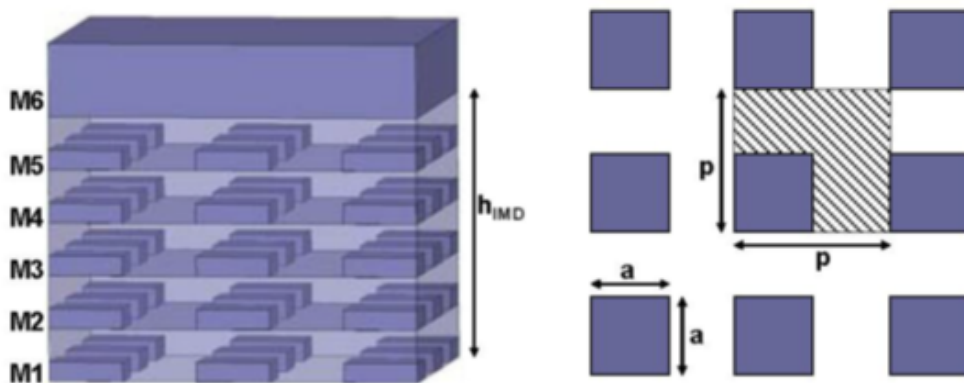
Figure 1.8.: Metal Fills
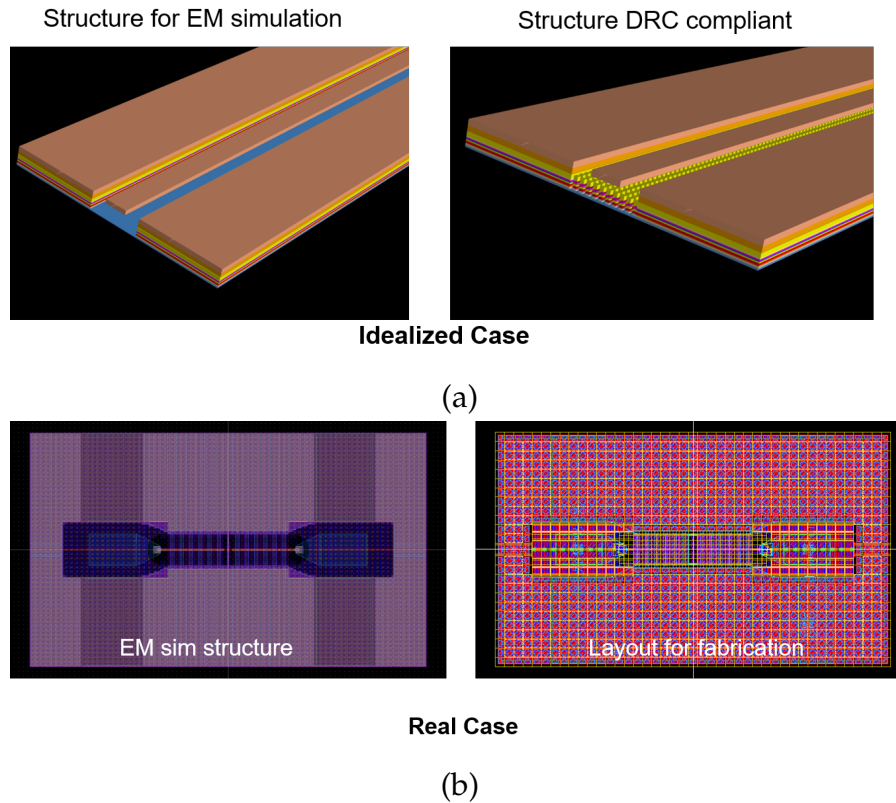
Figure 1.9.: (a) Structure - Ideal case (b) Structure - Practical case

necessitates the addition of the metal fills under RF structures depending on the technology, which makes their simulation exceedingly difficult.

1.3.2. Metal Fill Research Challenges

The performance of passive components, active components, interconnects and circuits are all impacted by the insertion of metal fillers. The following are the challenges faced while dealing with metal fills during the design phase:

i) Electrical parasitic effects: At high frequencies (several GHz), additional eddy-current loss in the metal fill can be detrimental to the properties of structures like inductors as well as circuit performance. At smaller technology nodes, the parasitic effect of metal fill is becoming more significant as density design restrictions are increasingly restricted and design criteria is more tight. Due to the performance reduction, it is crucial to take electromagnetic parasitic effects into account [16].

ii) Parasitic Extraction: Full parasitic capacitance extraction is impractical because of the substantial amount of metal fill injected in an area. Additionally, it is known that the metal fillings can cause accuracy issues with conventional capacitance extraction techniques. As a result, designers frequently make a variety of rough estimates or just ignore metal fill parasitics. Therefore, developing a quick, precise, and physically motivated interconnect and component extraction algorithms is difficult [9].

Hence, in this thesis work we will focus on the method that will take into account the effect of metal fills.

iii) Metal Fill Shape and Size: Ideal metal fill shape and size for a given structure layout is a challenging problem. It is important to optimize these metal fill parameters as well as electrical connections to reduce the impact of metal fill [1]. We will also discuss this problem and provide insights in this thesis work.

1.4. Thesis Contribution

1.4.1. Problem Statement

How to define a design flow methodology that takes into account the metal fills which has an impact on the performance of the structure at higher frequencies and also quantify the accuracy of 2.5D EM solvers with the help of 3D EM solver in order to incorporate as much as possible for various problems given by the design rule compliance and also reduce the simulation time.

1.4.2. Goal/Objective

The main goal is to develop a method which makes use of the EM tools that are already available in industrial design flow for IC design and layout, in order to compute an equivalent complex permittivity and permeability and delete the metal fill shapes from the layout and therefore take into account the influence of the metal fills and speed up EM simulations as shown in Figure 1.10.

The usage of the equivalent layer can be done quite accurately using 3D solvers where permittivity and permeability tensor can be employed, and is less accurate in 2.5D solver where only a scalar number can be provided. The objective of the thesis is also to understand all the possible limitations of 2.5D tools and provide approaches to extend the capability of 2.5D tools to improve accuracy which is fairly 3D complex.

Another important goal is to analyze the impact of different design aspects of metal fill such as feature alignment and shape. By using this approach, we can have a good approximation for the scalar number in order to enable 2.5D simulations with less error.
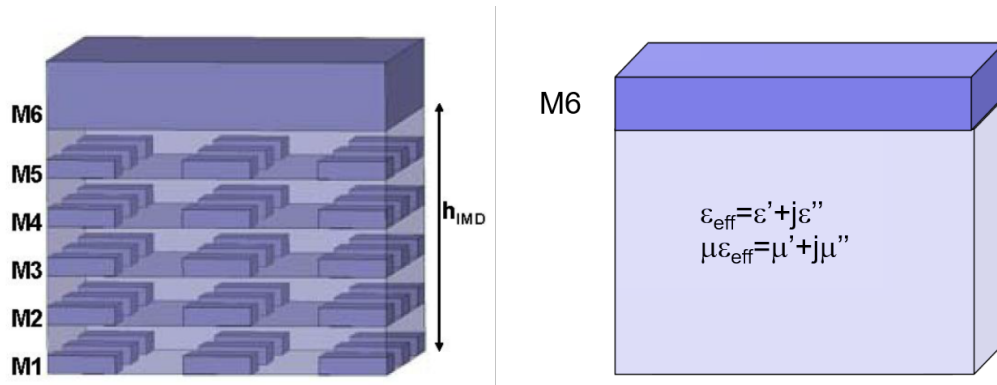
Figure 1.10.: Removing metal fills

1.5. Outline of the Thesis

- Chapter 1: The introduction and background information relevant to the subject of this thesis are the main topics. The thesis work's problem statement, goals and solution are outlined.

- Chapter 2: This chapter will focus on the Quasistatic Based Approach in order to extract the capacitance effects and its problems. This will be followed by the discussion about the State of Art solution which is the Oblique Incidence Method and its approximations.

- Chapter 3: A Design Flow Methodology will be presented and also a brief discussion about the Scalar Extraction Method will be presented. We will follow it up by quantifying this methodology with a simple example.

- Chapter 4: This chapter will provide the validation of the Design Flow Methodology by using two test cases which is the the wave propagating (Grounded Coplanar Waveguide) and lumped structure (Stacked Transformer).

- Chapter 5: This chapter deals with the Design Based Approach presenting the design of metal fills with different shapes and alignment. Finally, a test case is taken to verify and validate this approach.

- Chapter 6: A summary and conclusion of the thesis work along with recommendations for future research work will be provided.

2. Techniques to Extract RF Permittivity And Permeability Of Layers

This chapter describes two different approaches that can be used to extract the complex parameters providing the electromagnetic response of the layers, i.e. electrical permittivity and magnetic permeability. First, we describe the Quasistatic Approach to extract the epsilon parameters from the capacitance. After describing some of the limitations of this approach we will focus on the Oblique Incidence Method as reported in the literature.

2.1. Quasistatic Approximation Based Approach

In this section we present the procedure to extract the complex permittivity of a layer using Quasistatic field approximation. The method is based on the presence of an uniform electrical field in the dielectric present between the two plates of a parallel plate capacitor as shown in Figure 2.1. From the simple parallel plate capacitance formula, as will be shown in Section 2.1.1, we can derive the medium permittivity, i.e. ε_r.

2.1.1. Parallel Plate Capacitor

In this subsection, we will consider a parallel plate capacitor. Such a component can be constructed using two metal plates set at a fixed distance parallel to each other. The capacitance value is expressed in Farads and it is proportional to the surface area of the conductive plates (A) and the medium permittivity and is inversely proportional to the separation between them (d). The calculation of the capacitance can be done with the knowledge of the electric field intensity between the parallel plates and the permittivity as shown in following equations [17]:

The strength of the electric field E given the charge density ς on the plate

$$E = \varsigma/(\varepsilon_r \varepsilon_o) \tag{2.1}$$

where ε_o is the permittivity of vacuum, ε_r is the relative permittivity of the medium
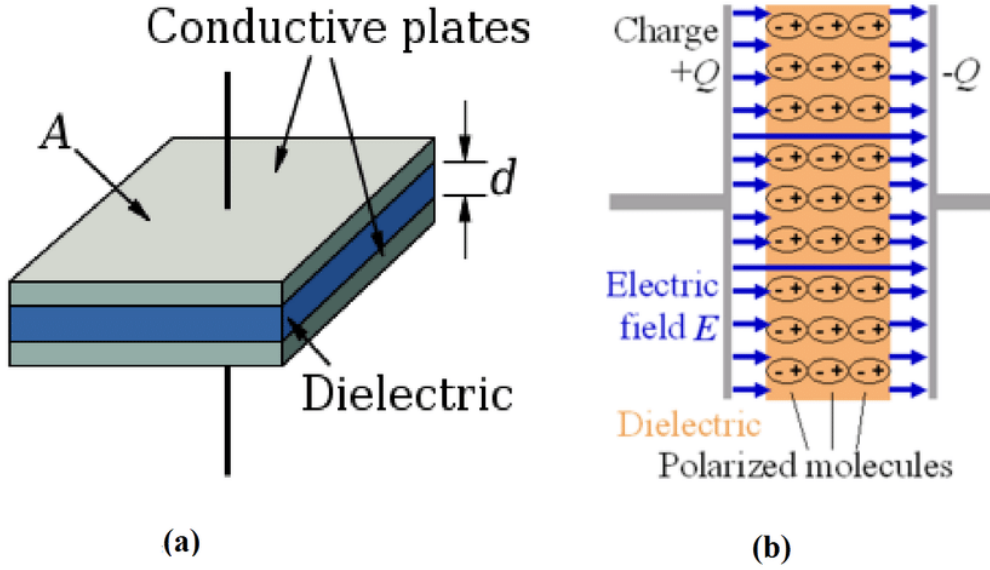
Figure 2.1.: (a) Capacitor with surface area and distance (b) Electric field between the parallel plates

If the plates have surface area A, they carry a total charge Q = ς A, then by using Equation 2.1,

$$Q = \varepsilon_r \varepsilon_o A E \tag{2.2}$$

Because the electric field is uniform in the dielectric, when the distance between the plates is d, then the voltage difference V between the plates is,

$$V = E/d \tag{2.3}$$

The capacitance C is defined as Q/V, and by making use of Equation 2.2 and Equation 2.3,

$$C = \varepsilon_r Co \tag{2.4}$$

where,

$$Co = \varepsilon_o A/d \tag{2.5}$$

Co is the capacity with vacuum between the plates.

Therefore, we can link the capacitance of a parallel-plate capacitor directly to the permittivity ε_r and thus express the latter as:

$$\varepsilon_r = Cd/\varepsilon_o A \tag{2.6}$$

When we consider losses in the dielectric, we can link the impedance (containing both reactive and conductive part) to the complex permittivity and conductivity as shown in Equation 2.7 [18].

$$Y = G + j\omega C = \left(\frac{A}{d}\right)(\sigma + j\omega\varepsilon) \tag{2.7}$$

13

Now from the complex impedance expression, we can find the capacitance as a complex number.

$$C_{complex} = (\frac{-1}{j\omega Z}) \tag{2.8}$$

Now, by using Equation 2.4 and Equation 2.5, we can extract the complex permittivity.

$$\varepsilon_{\mathrm{r}} = C_{complex}d/\varepsilon_{\mathrm{o}}A \tag{2.9}$$

Since the permittivity is a complex number, the imaginary part of the permittivity accounts for losses in the medium due to the damping of the vibrating dipole moments.

$$\varepsilon = \varepsilon' - j\varepsilon'' = (\varepsilon'_{\mathrm{r}} - j\varepsilon_{\mathrm{r}}'')\varepsilon_{\mathrm{o}} \tag{2.10}$$

2.1.2. Permittivity & Permeability Extraction from EM Simulation Tool

As discussed in the previous section, when the electric fields can be computed at each plate of a capacitor, we can derive the capacitance and then the permittivity can be extracted based on the dimension of the geometry.

For any given structure with a homogeneous dielectric or when it is composed with various floating metal elements (as would be the case when metal fill tiles are present) we can extract the electric fields on the plate of the capacitor by using an electrostatic or electromagnetic solver in one direction. In the example shown in Figure 2.2, an EM solver is considered where first, a homogeneous dielectric is inserted to test the procedure. As can be seen in the figure, the electric field is computed in every position of the 3D space, i.e. inside the meshed cell. By considering the area represented by the metal plate, the impedance can be computed and using the procedure described from Equation 2.8 to Equation 2.10, the capacitance and permittivity can be extracted.
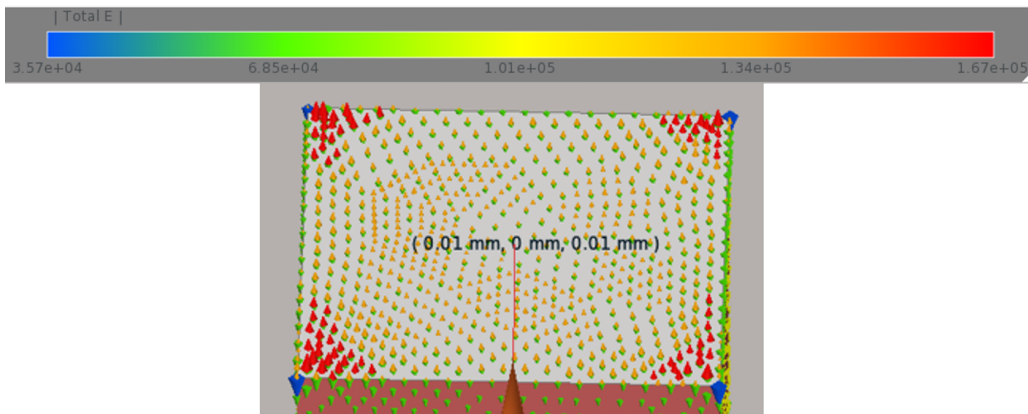
Figure 2.2.: Non uniform electric field distribution in parallel plate capacitor when employing in an EM solver

When considering the example of Figure 2.2, we note that the finite 3D structure will present discontinuities in space (i.e. at the edge of the plate where an air boundary will start) forcing the field to not be uniform.

Applying the procedure as mentioned above, by using the impedance to extract the capacitance and then the permittivity for a cube of lateral dimension of 20 micron, a known dielectric with ε_r of 4, we extract a capacitance value of 1.2357 fF. When using the geometrical values to compute the permittivity (i.e. by taking the ratio of C/C0), we obtain a value of 6.9782, representing an error of 74.42%. The reason for this is found to be in the non uniformity of the field in the edges of the cube as seen in Figure 2.2. A way to overcome this problem would be to analyze only a part of the structure far away from the edges as shown in Figure 2.3 represented by the black region. The field shown in the black region represents a good uniformity in the electric field ranging from 5.17e+04 to 5.19e+04. Since the variation in the electric field is less, the permittivity value can be extracted correctly.
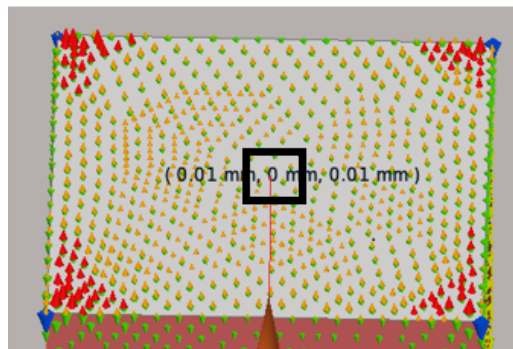
Figure 2.3.: Structure far away from edges

In order to extract the capacitance value from the simulator avoiding the edge effects, we can have a set of boundary conditions which approximates the structure to be infinitely large and these are often called as periodic boundary conditions. The way to implement them in modern EM simulator will be explained in detail in Chapter 3. Using this setting, the edge effects are not present and hence the variation of the electric field is small as shown below in Figure 2.4. By repeating the analysis as before to extract the capacitance and permittivity, we observe a capacitance value of 0.7083 fF and the correct permittivity value of 4 which matches the host dielectric medium set in the simulator. This simulation should be repeated across the three axes to extract a diagonal permittivity behavior.

2. Techniques to Extract RF Permittivity And Permeability Of Layers
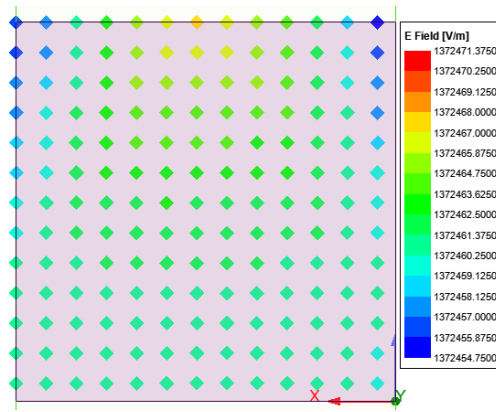
Figure 2.4.: Uniform field using periodic boundary condition

To extract the permeability using Quasistatic Approach, instead of a metal plate we need to use a structure which can generate an uniform magnetic field, thus creating the dual case of the capacitor as shown in Figure 2.5.

$$\phi = \int_S \mathbf{B} \cdot d\mathbf{s} = \mu J_s l d = \frac{\mu l d}{w} I \qquad \boxed{L = \frac{\mu l d}{w}}$$
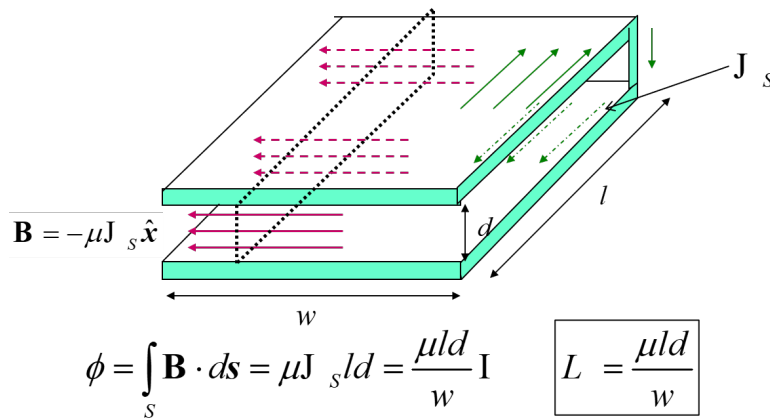
Figure 2.5.: Metal sheet to generate uniform magnetic field in order extract inductance

This case can then be simply realized using a metal sheet which can allow us to extract the vacuum inductance from the geometrical values and from comparison with the EM extracted inductance we can compute the relative permeability μr in the direction of the uniform field. The calculation of the inductance can be done with the knowledge of the magnetic field intensity and the permeability as shown in following equations:

The Magnetic field strength H is related to the Magnetic flux density B,

$$H = B/\mu_0 \mu_r \qquad (2.11)$$

16

The Magnetic flux density B using the surface current density J_s is,

$$B = -\mu J_s \tag{2.12}$$

The Magnetic flux density is defined as,

$$B = \phi/A \tag{2.13}$$

By integrating the flux over an area A we get,

$$\phi = \int_A B.\, dA = \mu_o \mu_r J_s A = \frac{\mu_o \mu_r A I}{d} \tag{2.14}$$

The inductance of the metal sheet is defined as,

$$L = \phi/I \tag{2.15}$$

By using Equation 2.14 and Equation 2.15

$$\mu_r = Ld/\mu_o A \tag{2.16}$$

Similar to the capacitor case, by linking the inductance term to the impedance we get the complex term,

$$L_{complex} = \frac{Z}{j\omega} \tag{2.17}$$

Now applying the complex term to Equation 2.16, we get

$$\mu_r = L_{complex} d/\mu_o A \tag{2.18}$$

By applying the procedure as mentioned above and by using the impedance to extract the inductance and then the permeability of the metal sheet for a cube of lateral dimension of 20 micron as shown below in Figure 2.6 , we extract an inductance value of 0.0251 nH. When using the geometrical values to compute the permeability, we obtain a permeability value of 1.
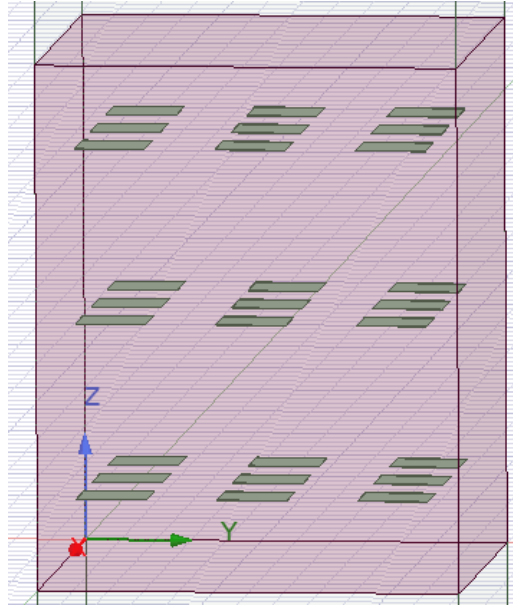
Figure 2.6.: Metal sheet to generate uniform magnetic field to extract permeability in EM solver

After this brief review of the electrostatic and magnetostatic approaches to extract μ and ε for a bi-anisotropic it can be see that multiple simulations using different reference structures (i.e. capacitor and metal sheet) needs to be employed under different excitations. This makes the approach less direct in it's implementation in an automated design flow to support integrated circuit designs. For this reason a different approach based on the relation of the material properties with the reflection and transmission coefficient of incident fields under different angles will be considered and detailed in the next section.

2.2. Oblique Incidence Method

The general approach for the extraction of the effective permittivity and permeability is by using the Scattering Parameters (S Parameters) of a plane incident wave from the material and this has been analysed and evaluated in several papers [19–26].

It was shown in [26] that a generic layer with metal fill inclusion can be represented by using a bianisotropic homogeneous medium. The bianisotropic homogeneous medium is a pseudochiral omega medium and assumed to have diagonal permittivity and permeability tensors related to the fields [25] as shown below.

$$D = \bar{\bar{\varepsilon}}E,$$

$$B = \bar{\bar{\mu}}H$$

(2.19)

The metal fills creates an analogous material that can be described by its effective properties, namely permittivity and permeability. This allows to model the metal fills as an equivalent homogeneous, anisotropic slab with a finite height [25]. Hence the effective permittivity and permeability is represented by second ranked tensor behavior $\bar{\bar{\varepsilon}}, \bar{\bar{\mu}}$ as shown in Figure 2.7.

$$\bar{\bar{\varepsilon}} = \varepsilon_0 \begin{pmatrix} \varepsilon_x & 0 & 0 \\ 0 & \varepsilon_y & 0 \\ 0 & 0 & \varepsilon_z \end{pmatrix}, \qquad \bar{\bar{\mu}} = \mu_0 \begin{pmatrix} \mu_x & 0 & 0 \\ 0 & \mu_y & 0 \\ 0 & 0 & \mu_z \end{pmatrix}$$

Figure 2.7.: Tensor Behavior

where,

ε_o - Permittivity of free space

μ_o - Permeability of free space

ε_x - Unknown Permittivity tensor (x direction)

ε_y - Unknown Permittivity tensor (y direction)

ε_z - Unknown Permittivity tensor (z direction)

μ_x - Unknown Permeability tensor (x direction)

μ_y - Unknown Permeability tensor (y direction)

μ_z - Unknown Permeability tensor (z direction)

The method described in [25] as mentioned takes into account a bianisotropic slab made up of thickness (d) where the plane wave is obliquely incident as shown in Figure 2.8, and the unknown effective permittivity and permeability tensors are obtained using the S Parameters that are derived from the normal and oblique incidence for the vertical (TE) and horizontal (TM) components and are shown below in the following equations.
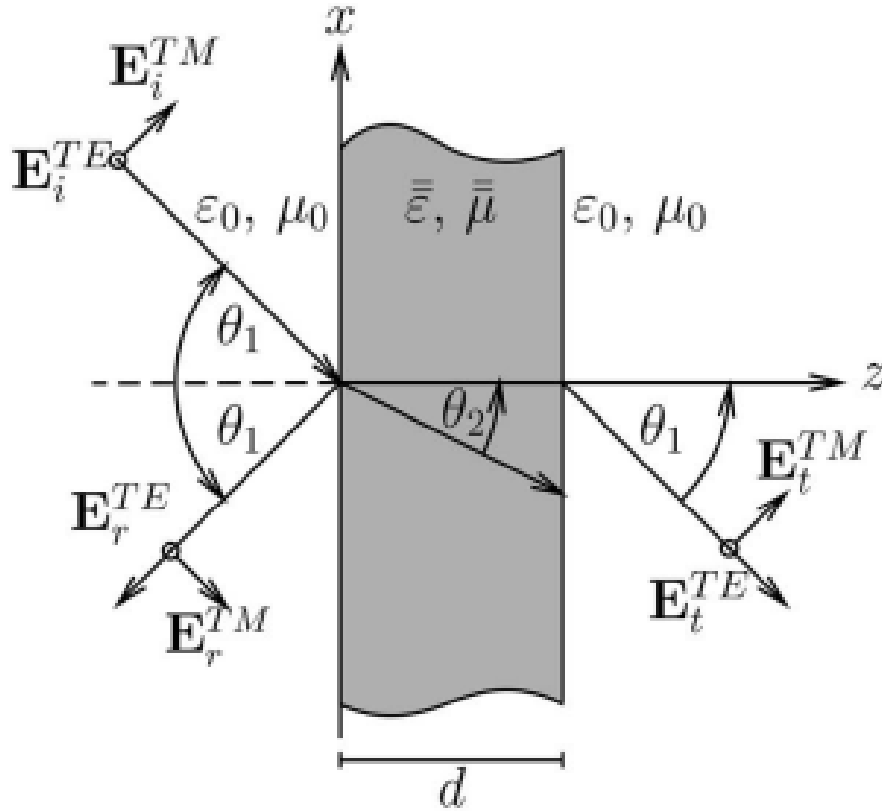
Figure 2.8.: Geometry of the slab

The S Parameters are derived from the elements of the reflection $\overline{\overline{R}}$ and transmittance $\overline{\overline{T}}$ matrices. The elements of the main diagonal represent the S Parameters due to TE and TM incidence and the off diagonal elements represent the scattering coefficient of TE due to incident TM and vice versa.

$$\overline{\overline{R}} = \begin{pmatrix} S_{11}^{TM} & S_{11}^{TE,TM} \\ S_{11}^{TM,TE} & S_{11}^{TE} \end{pmatrix} \tag{2.20}$$

$$\overline{\overline{T}} = \begin{pmatrix} S_{21}^{TM} & S_{21}^{TE,TM} \\ S_{21}^{TM,TE} & S_{21}^{TE} \end{pmatrix} \tag{2.21}$$

$$S_{11}^{TM} = \frac{\Gamma^{TM}(1 - e^{-j2k_z^{TM}d})}{1 - (\Gamma^{TM})^2 e^{-j2k_z^{TM}d}},$$

$$S_{11}^{TE} = \frac{\Gamma^{TE}(1 - e^{-j2k_z^{TE}d})}{1 - (\Gamma^{TE})^2 e^{-j2k_z^{TE}d}},$$

$$S_{21}^{TM} = \frac{(1 - (\Gamma^{TM})^2)e^{-jk_z^{TM}d}}{1 - (\Gamma^{TM})^2 e^{-j2k_z^{TM}d}},$$

$$S_{21}^{TE} = \frac{(1 - (\Gamma^{TE})^2)e^{-jk_z^{TE}d}}{1 - (\Gamma^{TE})^2 e^{-j2k_z^{TE}d}}$$

(2.22)

where the reflection coefficient Γ^{TE} and Γ^{TM} are represented as,

$$\Gamma^{TM} = \frac{\eta^{TM}/cos\theta_1 - 1}{\eta^{TM}/cos\theta_1 + 1},$$

$$\Gamma^{TE} = \frac{\eta^{TE}/cos\theta_1 - 1}{\eta^{TE}/cos\theta_1 + 1},$$

$$\eta^{TM} = \sqrt{(\mu_y - (sin^2\theta_1 + \xi_0^2)/\varepsilon_z)/\varepsilon_x},$$

$$\eta^{TE} = \sqrt{\mu_x/(\varepsilon_y - sin^2\theta_1/\mu_z)}$$

(2.23)

and wave number in the z direction for TE and TM polarization are

$$k_z^{TM} = k_0 n^{TM} cos\theta_2,$$

$$k_z^{TE} = k_0 n^{TE} cos\theta_2,$$

$$n^{TM} = \sqrt{\varepsilon_x\mu_y + (1 - \varepsilon_x/\varepsilon_z sin^2\theta_1 - (\varepsilon_x/\varepsilon_z)\xi_0^2},$$

$$n^{TE} = \sqrt{\varepsilon_y\mu_x + (1 - \mu_x/\mu_z)sin^2\theta_1}$$

(2.24)

By using the derived S Parameters as shown in Equation 2.22 for the TE and TM polarization, the unknown effective epsilon permittivity and permeability parameters can be extracted at normal and oblique incidence.

2. Techniques to Extract RF Permittivity And Permeability Of Layers

The wave impedance η and refractive index n in terms of the S Parameters is represented as,

$$\eta^{TE} = \pm\sqrt{\frac{(1 + S_{11}^{TE})^2 - (S_{21}^{TE})^2}{(1 - S_{11}^{TE})^2 - (S_{21}^{TE})^2}}sec\theta_1,$$

$$\eta^{TM} = \pm\sqrt{\frac{(1 + S_{11}^{TM})^2 - (S_{21}^{TM})^2}{(1 - S_{11}^{TM})^2 - (S_{21}^{TM})^2}}cos\theta_1,$$

(2.25)

$$n^{TE} = \sqrt{\left[\frac{log|\varsigma^{TE}| + j(\angle(\varsigma^{TE}) + 2\pi m)}{-jk_0d}\right]^2 + sin^2\theta_1},$$

$$n^{TM} = \sqrt{\left[\frac{log|\varsigma^{TM}| + j(\angle(\varsigma^{TM}) + 2\pi\overline{m})}{-jk_0d}\right]^2 + sin^2\theta_1},$$

(2.26)

where m and $\overline{m}$ are independent integers,

$$\varsigma^{TE} = \frac{S_{21}^{TE}}{1 - S_{11}^{TE}(\eta^{TE}cos\theta_1 - 1)/(\eta^{TE}cos\theta_1 + 1)},$$

$$\varsigma^{TM} = \frac{S_{21}^{TM}}{1 - S_{11}^{TM}(\eta^{TE}/cos\theta_1 - 1)/(\eta^{TE}/cos\theta_1 + 1)},$$

(2.27)

All the equations are dependent on the normal incidence and oblique incidence,

$$\varepsilon_x = n^{TM}/\eta^{TM}|_{\theta_1=0},$$

$$\varepsilon_y = n^{TE}/\eta^{TE}|_{\theta_1=0},$$

(2.28)

$$\mu_x = n^{TE}\eta^{TE}|_{\theta_1=0},$$

$$\mu_y = n^{TM}\eta^{TM}|_{\theta_1=0},$$

(2.29)

The ε_x, ε_y, μ_x, μ_y parameters are ambiguous because the independent integers m and $\overline{m}$ are not yet known. The vertical constitutive parameters ε_z, μ_z are extracted by utilizing both Equation 2.23 and Equation 2.24. By using the extracted parameters in Equation 2.28 and Equation 2.29 , the following sets of equations for the vertical

component as a function of the branch indices m and $\overline{m}$ at normal and oblique incidence are derived.

$$
\begin{aligned}
\varepsilon_z^{(1)} &= \varepsilon_x sin^2\theta_1 / (sin^2\theta_1 - (n^{TM})^2 + (n^{TM})^2|_{\theta_1=0}), \\
\mu_z^{(1)} &= sin^2\theta_1 / ((n^{TE}/\eta^{TE})|_{\theta_1=0} - \mu_x/(\eta^{TE})^2), \\
\varepsilon_z^{(2)} &= sin^2\theta_1 / ((n^{TM}\eta^{TM})|_{\theta_1=0} - \varepsilon_x(\eta^{TM})^2), \\
\mu_z^{(2)} &= \mu_x sin^2\theta_1 / (sin^2\theta_1 - (n^{TE})^2 + (n^{TE})^2|_{\theta_1=0}),
\end{aligned}
\tag{2.30}
$$

The two sets of vertical parameters are equated to acquire the right branch indices m and $\overline{m}$ as shown below and once the right branch indices are obtained, the epsilon permittivity and permeability components become unambiguous and the results can be explicitly obtained.

$$
\begin{aligned}
\varepsilon_z^{(1)}(\overline{m}) &= \varepsilon_z^{(2)}(\overline{m}), \\
\mu_z^{(1)}(m) &= \mu_z^{(2)}(m),
\end{aligned}
\tag{2.31}
$$

This method has been adopted in the thesis work due to its advantage of extracting all the effective parameters of the equivalent dielectric slab. This method also shows that it can be effectively used in modern commercial EM simulation tools and can be embedded in the design flow process without requiring multiple simulations.

The Terahertz Sensing Group developed a metal fill tool also known as ADL tool which makes use of the above method but it doesn't account for the thickness of the metal fills. This tool takes the metal fill geometry as input and provides the epsilon permittivity and permeability tensors as output. Figure 2.9 shows a snippet of the ADL tool. The ADL tool will be used in the next chapter to benchmark the material parameters from the EM tool where infinitely thin metal layers are considered.
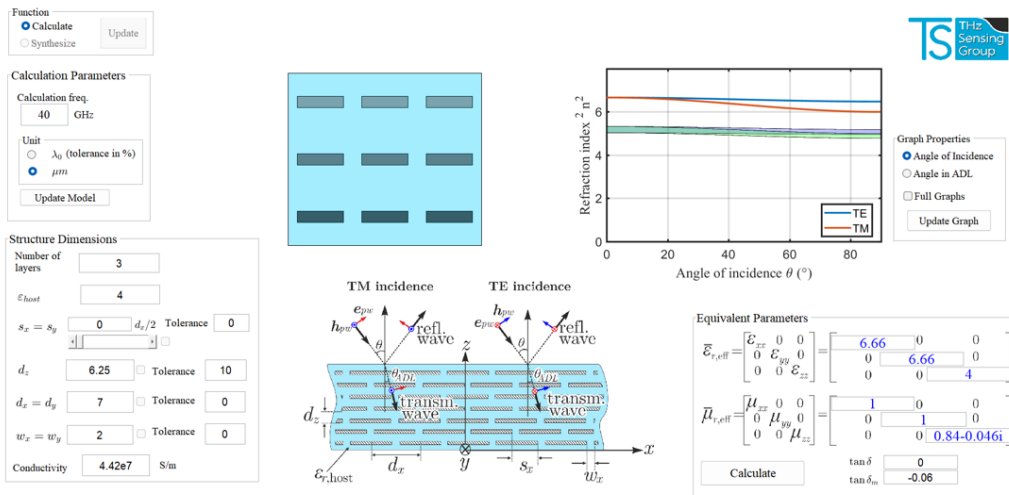
Figure 2.9.: ADL Tool

We will see in the next chapter as to how this method is incorporated in a design flow with the commercial EM solvers and MATLAB routines to extract permittivity and permeability.

2.2.1. Discussion/Conclusion

It was seen that the Quasistatic Approach for the parallel plate capacitor did not give accurate results for the permittivity due to the edge effects which was present, but when we use periodic boundary condition, we see that the edge effect becomes negligible and the permittivity matches that of the dielectric medium. But this simulation needs to be repeated in three axes to extract the diagonal permittivity behavior. The permeability extraction using Quasistatic Approach would require a structure with a series current flowing to compute the magnetic field and extract the inductance parameter and therefore the permeability of the structure. Hence, from this it is seen that the Quasistatic Approach would require two different structures to compute the permittivity and permeability and therefore multiple simulations would be required. The Oblique Incidence S Parameters Method proposed in the literature is based on the concept that a single structure can instead provide the same set of information based on the reflection coefficient provided by a TE and TM excitation under two angle of incidences (normal and oblique) and this would limit the number of simulations to be run and hence makes the approach more efficient for embedding in the design flow. With this method, infinitely repeated replicas of basic cells can be used that can be mapped easily in modern 3D simulator to avoid the edge effects. This method will be used in the thesis work because of its benefit that the effect of metal fills can be considered as complex permittivity and permeability with the advantage of reduced simulation time.

3. Design Flow Methodology

In this chapter, first we will focus on the description of Unit Cell Approach using Floquet ports that makes use of the Oblique Incidence Method mentioned in the previous chapter to extract the effective epsilon parameters for the metal fills. The validation of this approach is done for i) Homogeneous material, ii) Anisotropic material and iii) for the metal fill inclusion in the dielectric. This is followed by the description on how to embed the Obique Incidence solution present in section Section 2.2 in a design flow with 3D EM solver and MATLAB script. Then, a discussion on the impact of thick metal layers of the Oblique Incidence Method versus the ADL tool which uses metal layers of zero thickness is provided. Finally, an insight of how the solution from the Oblique Incidence Method can be used to extract a scalar number for the effective parameters and therefore be implemented in 2.5D EM tools.

3.1. Unit Cell Approach Using Floquet Ports

Unit cell is the repetition of the modeled structure periodically in two directions up to infinity. The ports define where the signal moves into and out of the simulation space and the Floquet port is particularly used for planar periodic structures. The metal fills are assumed to be idealized as infinitely large arrays where each element (metal fill) is physically and electrically the same [27]. The study of a Unit Cell is then used to complete the analysis of the infinite structure as shown in Figure 3.1

The metal fill is a periodic structure that requires an infinite repetition of the unit element in the direction of the lattice vectors. There are two types of boundary conditions that are used to achieve the periodicity. First is the combination of Perfect Electric and Perfect Magnetic boundary conditions. Another boundary condition is the Floquet boundary conditions provided by HFSS (i.e. two pairs of Primary and Secondary Boundaries) as shown below in Figure 3.2. This enables to model the planes of periodicity where they force the electric field at each point on one surface (Secondary) and match the electric field within a "phase difference" at each corresponding point on the other surface (Primary) as shown in Figure 3.3, hence realizing an infinite periodic condition and this boundary condition will be used in the thesis work with a phase difference of $30°$[27].
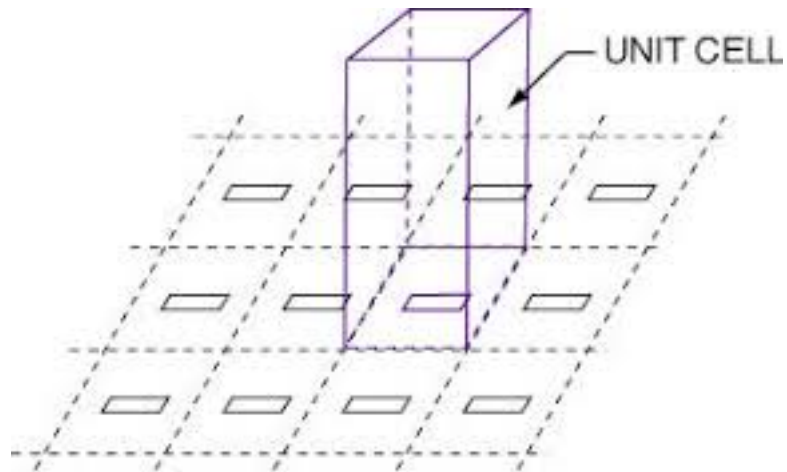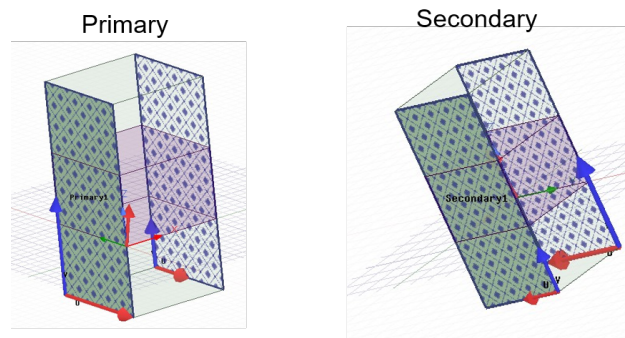
Figure 3.1.: Unit cell

Figure 3.2.: Primary and Secondary Boundaries
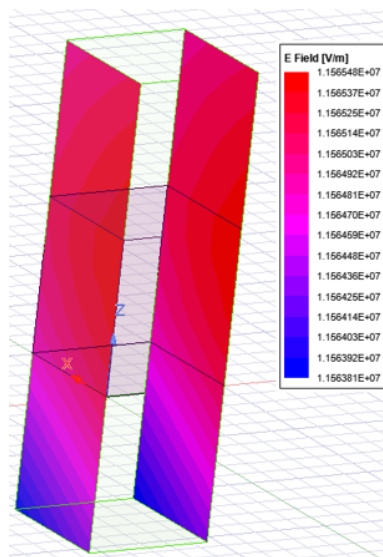
Figure 3.3.: Electric fields that match primary and secondary boundary conditions

Once the boundary conditions are set, the excitation ports are used to excite the structure. The Floquet ports directs the incident wave to propagate from the top to bottom and vice versa of the unit element as shown in Figure 3.4. Figure 3.5 shows the fields on the port boundary which are represented by a set of modes known as Floquet modes. Primarily, Floquet modes (i.e. TE,TM modes) are planar waves whose propagation direction is determined by the periodic structure's phase, geometry and periodicity[28],[29].
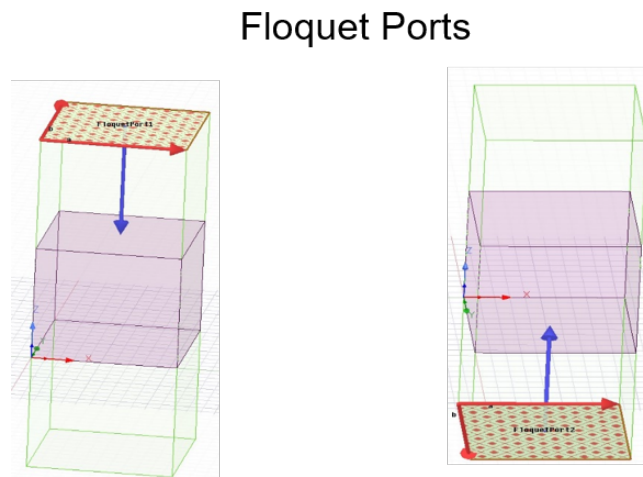
Figure 3.4.: Floquet Ports
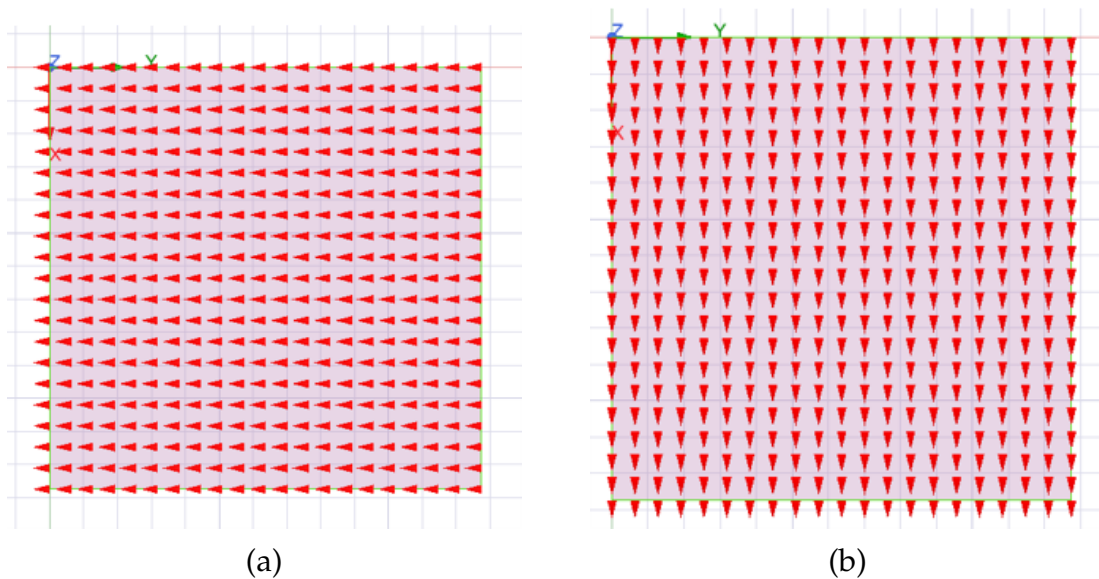
Figure 3.5.: (a) Horizontal component (TM) (b) Vertical component (TE)

The Unit Cell analysis is done for the periodic structures by using the Floquet boundary condition and Floquet ports. In order to make the metal fill structure periodic in an unit cell, half the spacing of the metal fills at each end has to be considered. The Unit Cell Approach enables the Oblique Incidence Method described in Section 2.2 to extract effective epsilon parameters using S Parameters for Vertical (TE) and Horizontal (TM) components at both the oblique and normal incidence.

3.1.1. Validation Of Oblique Incidence Method Using Unit Cell Approach

In this section, we will validate the Oblique Incidence Method mentioned in Section 2.2 that makes use of the Unit Cell approach for i) Homogeneous material, ii) Anisotropic material and iii) with the metal fill inclusion in the dielectric by having the ADL tool as the reference developed by the Terahertz Sensing group. We will consider a 15 micron substrate (height) with the airbox distance of $\lambda/4$ from the substrate for all the cases.

i) **Validation of Homogeneous material:** A homogeneous material is uniform in all directions and epsilon permittivity of 4 and epsilon permeability of 1 is considered in the 3D EM simulation tool. Applying the Floquet boundary condition and Floquet port to the structure as presented in the last section and using the Oblique Incidence Method mentioned in Section 2.2 for the TE and TM components at normal and oblique incidence and by using Equation 2.25 to Equation 2.31, we can extract the permittivity and permeability. Figure 3.6a and Figure 3.6b shows that both the permittivity and permeability matches that of the homogeneous material given in the simulation tool and hence validates the method.

ii) **Validation of Anisotropic material:** Similar to the homogeneous case, when we place the dielectric with anisotropic behavior in the 3D EM simulation tool (i.e. epsilon permittivity and permeability is direction dependent) with $\varepsilon_x = 3$, $\varepsilon_y = 4$, $\varepsilon_z = 5$ and $\mu_x = 1$, $\mu_y = 0.7$, $\mu_z = 0.5$ and follow the same procedure as the above case by applying the boundary condition and the Floquet ports, we extract the permittivity and permeability using the Oblique Incidence Method. From the below Figure 3.7a and Figure 3.7b, we see that they match the given anisotropic material and therefore we can validate for the case of the anisotropic material as well.
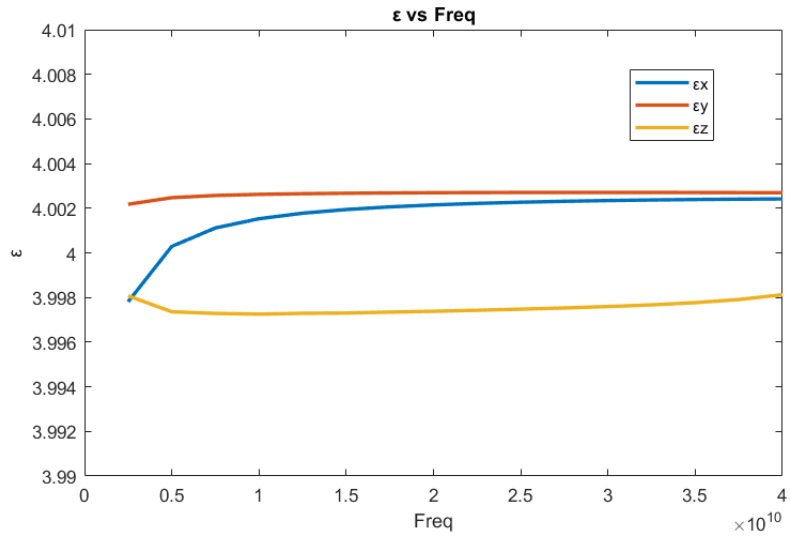
(a)
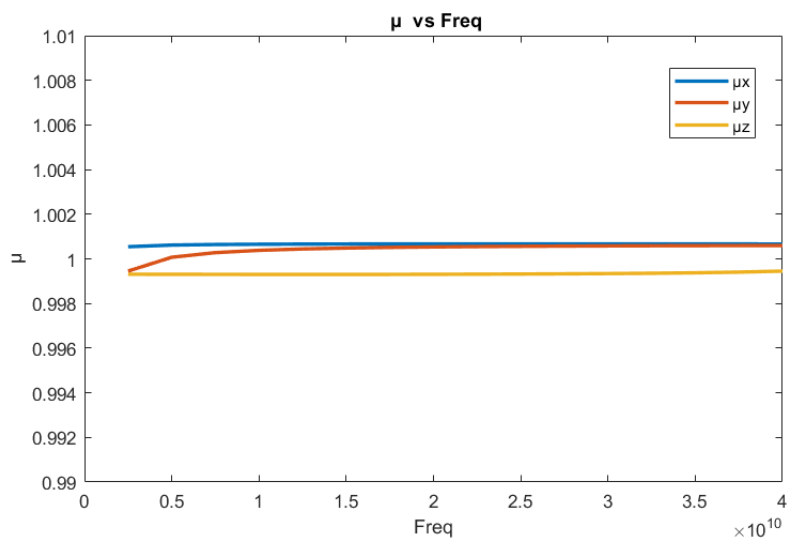
(b)

Figure 3.6.: (a) Epsilon Permittivity (b) Epsilon Permeability
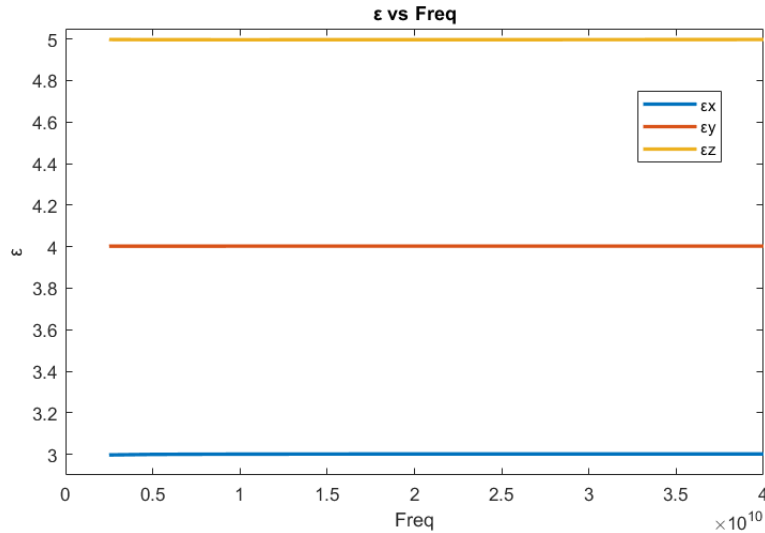
(a)
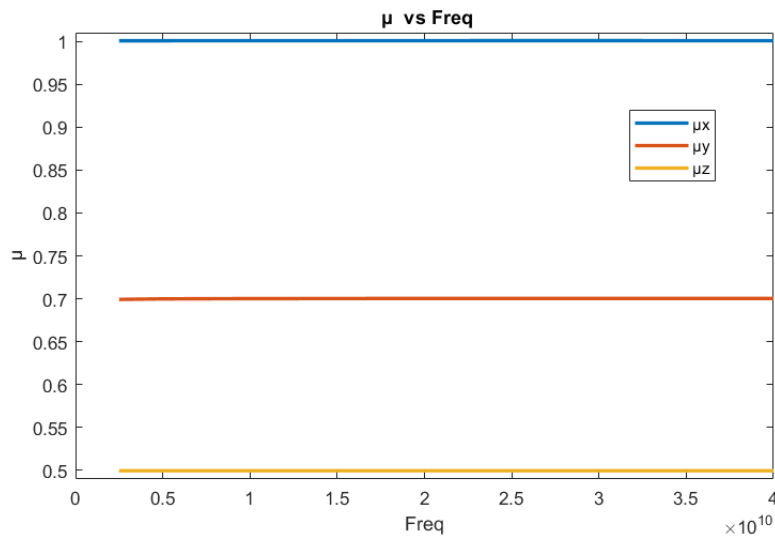
(b)

Figure 3.7.: (a) Epsilon Permittivity (b) Epsilon Permeability

iii) **Validation of Metal Fill inclusion in dielectric:** For the metal fill case, dielectric (host medium) with epsilon permittivity of 4 and epsilon permeability of 1 is considered in the 3D EM simulation tool and the metal fill thickness of 0.001 micron is chosen (almost zero thickness) to provide material properties like conductivity to the metal fills. The ADL tool which takes the geometrical parameters as input and gives epsilon permittivity and permeability tensors as output is taken as a reference which considers zero thickness for the metal fills. By following the same procedure as the above cases for the boundary conditions and Floquet ports, we can extract the permittivity and permeability using the Oblique Incidence Method as shown in Figure 3.8a and Figure 3.8b . Due to the inclusion of the metal fills, it can be seen that the permittivity components ε_x and ε_y increases with respect to the host medium of

3.1. Unit Cell Approach Using Floquet Ports

epsilon permittivity of 4 because of the mutual capacitance between layers and ε_z remains the same value of the host dielectric because the electric field does not come in contact in the vertical direction of the metal fill. The permeability component μ_z shows that it is always less than 1 showing that the diamagnetic property is seen in the z direction of the metal fills. This shows that the produced magnetic field is opposite to the direction of incidence magnetic field. Permeability components μ_x and μ_y is close to 1.
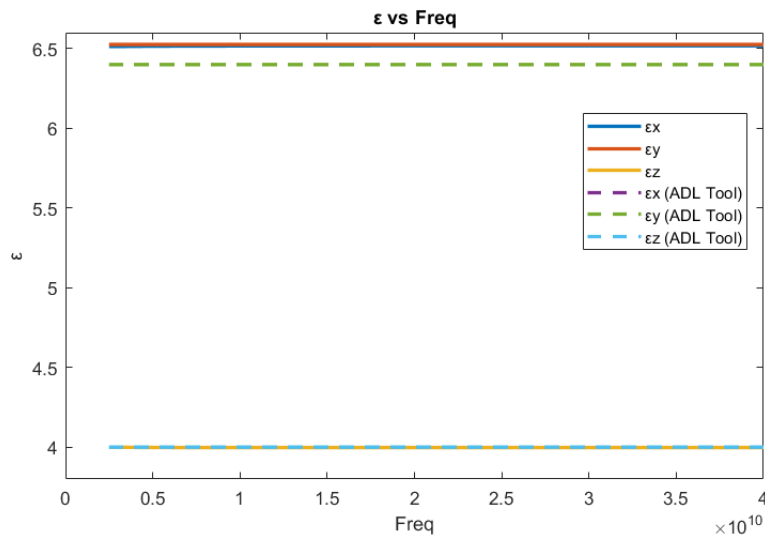
(a)
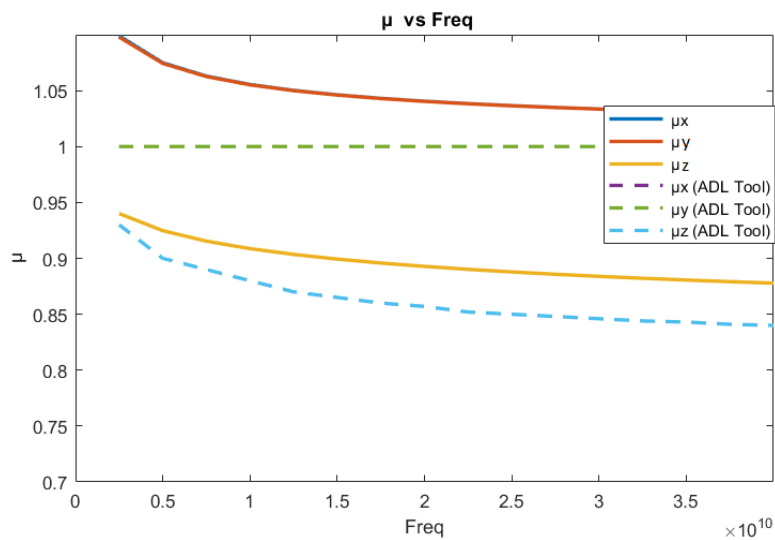
(b)

Figure 3.8.: (a) Epsilon Permittivity (b) Epsilon Permeability

31

3.2. Embedding the Oblique Incidence Method in Design flow

This section will show the entire design flow from designing the metal fill structure in 2.5D EM tool (Cadence Virtuoso EMX) and translating the design to the 3D EM tool (HFSS) by making use of the GDS file, Technology files and Layer map files. We will also see how the Oblique Incidence Method seen in Section 2.2 is embedded into the design flow in order to take into account the effect of metal fills before the entire design goes for final DRC check and therefore the fabrication step.

3.2.1. Design Flow

Step 1: Design the metal fill structure in Cadence Virtuoso EMX which is a 2.5D EM tool shown in Figure 3.9
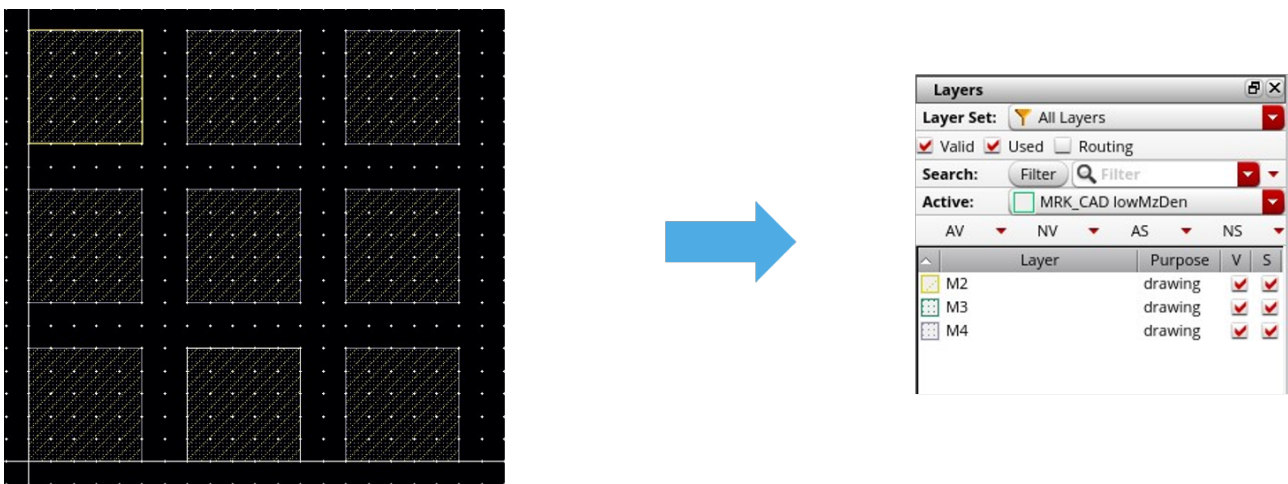
Figure 3.9.: Step 1 - Design metal fill structure in 2.5D EM tool (Virtuoso EMX)

Step 2: Creating the GDS file for the metal fill structure. GDS file contains information about the layout of a circuit, including the layers, geometric shapes and text labels and hence used as a standard interchange format between IC design applications, for instance as shown in Figure 3.10. Therefore, this file helps to translate the structure to 3D EM tool.

Figure 3.10.: Step 2 - Creating GDS file

Step 3: Another important file is the Technology file that contains information such as technology name, units etc. Definition of a different colour with RGB values for each layer is visible in the layout. All metal layers and via information along with design rules such as width (min-max), min spacing, area(min-max), pitch, colour, max current density is provided. Along with metal layers, physical profile information regarding diffusion layer and polysilicon layer is also given. Via related information like colour, layers, patterns, min-width, min spacing, pitch and max current density is specified. Layer map file plays a key role that presents details on how to map between layers in a Cadence layout and layers in a GDS file. This file plays an important role in translation of the structure to the 3D EM tool which is HFSS 3D Layout.

Step 4: Figure 3.11 shows how the above mentioned files (GDS, Technology and Layermap) will aid to import the structure in HFSS 3D layout tool.
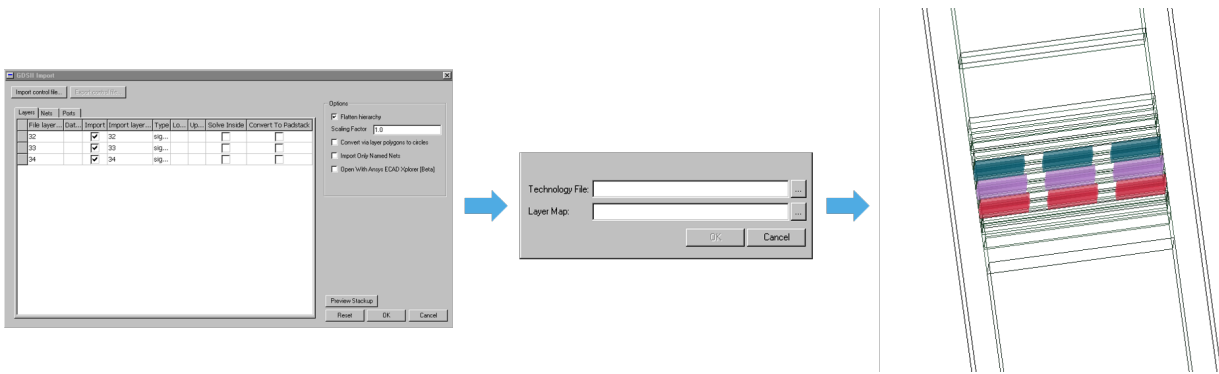
Figure 3.11.: Step 4 - Importing the structure in HFSS 3D layout

Step 5: Now that the structure is imported from 2.5D tool (Cadence Virtuoso EMX) to 3D tool (HFSS 3D Layout) with all the necessary files, the next step is to define an airbox for the structure. An airbox has to be defined so that the radiation from the structure is absorbed and not reflected back. The airbox should be a quarter-wavelength from the edge of the design. In the airbox wizard extent present in the HFSS 3D layout shown in Figure 3.12, we have the option to mention the horizontal padding for the dielectric (i.e. spacing on each end of the dielectric) and generally half the spacing on each side of the structure should be given since we have to make the metal fills as an unit cell which is periodic in nature.
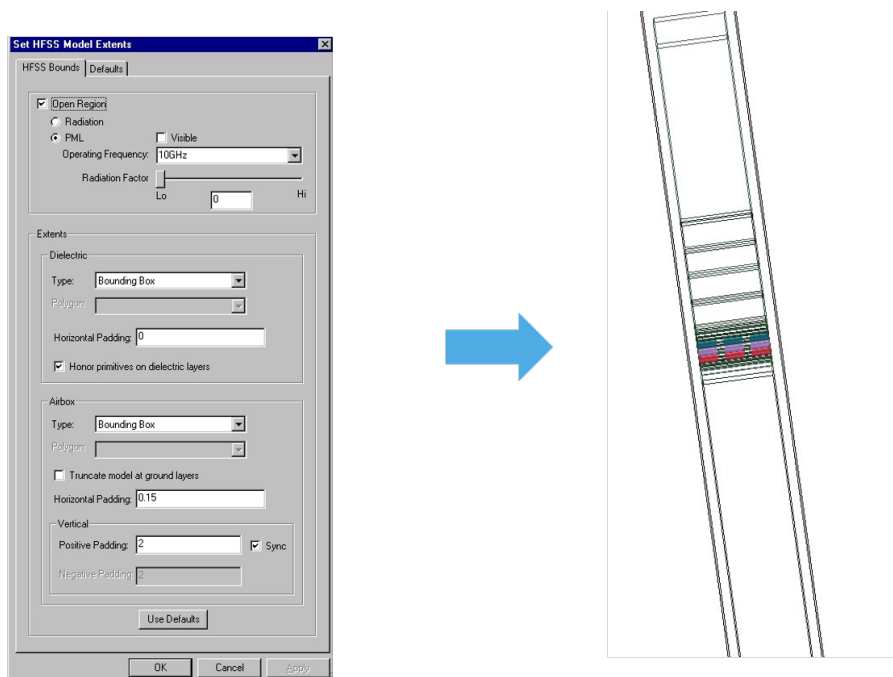
Figure 3.12.: Step 5 - Airbox Extent

Step 6: With the airbox being placed, we now have to make sure that the simulation analysis is setup in order to export the metal fill structure to HFSS Modeller. In HFSS Modeller, the classic meshing technique is used which uses 3D surface triangular mesh on all objects and generates a 3D volume mesh. In order to embed the Oblique Incidence Method in the design flow, HFSS Modeller is used.

(a)   (b)
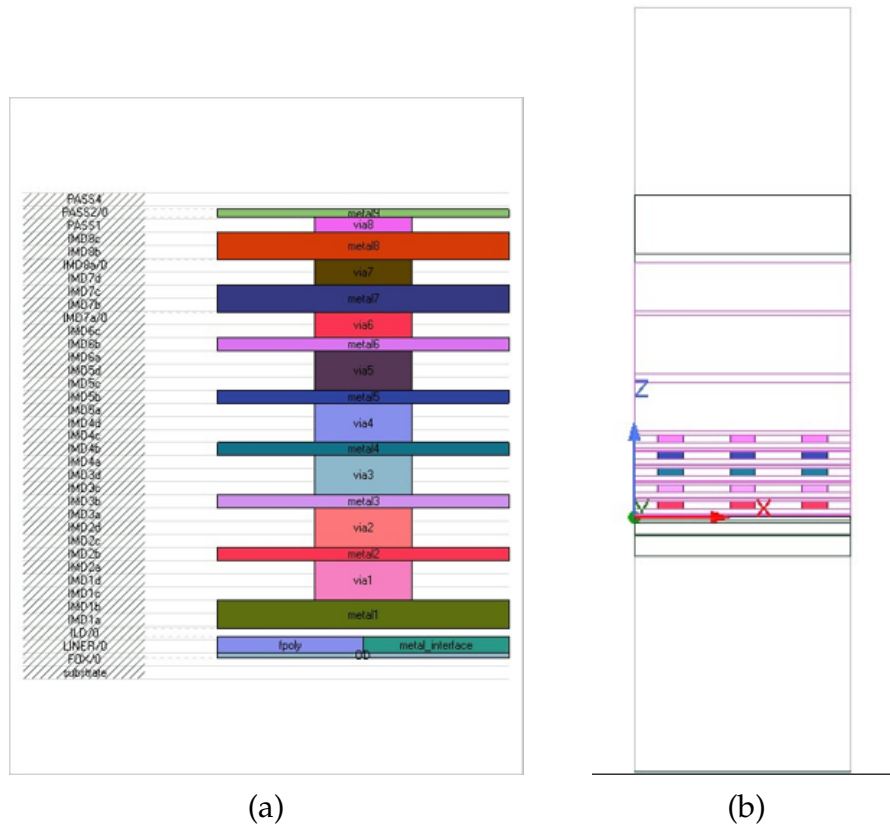
Figure 3.13.: (a) Metal layers with the dielectric . (b) Metal fills in HFSS Modeller.

Step 7: Now that the metal fill structure is exported to HFSS Modeller as illustrated in Figure 3.13, we will apply the Unit Cell Approach using the Floquet ports for the metal fill structure as mentioned in the last section. Both the Floquet boundary conditions as shown in Figure 3.14 and Floquet ports seen in Figure 3.15 is applied at normal and oblique incidence that make use of vertical (TE) and horizontal (TM) components. In this thesis, the oblique incidence angle that was chosen is 30°.
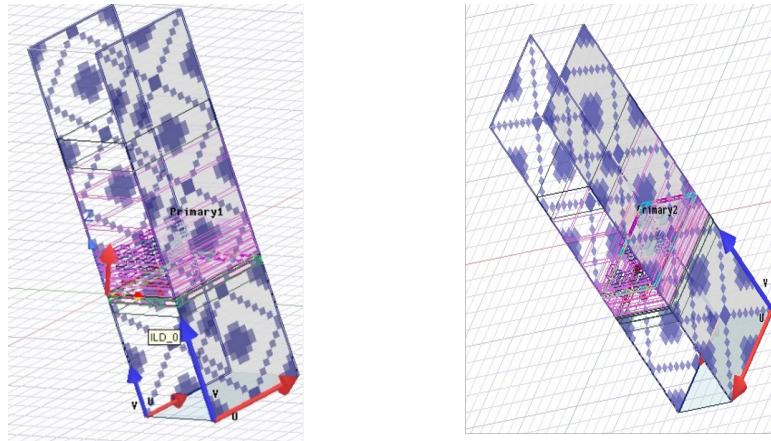
Figure 3.14.: Step 7 - Boundary Condition
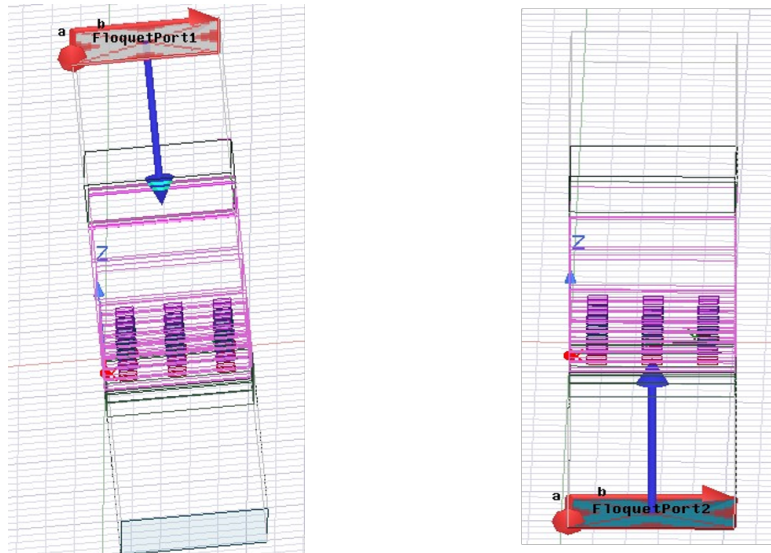
Figure 3.15.: Step 7 - Floquet Ports

Step 8: Now that everything is set up, the next step is to export the S Parameters results for both the excitation and place the values in the MATLAB script as shown in the Appendix (Section A.1) that uses Equation 2.25 to Equation 2.31 to extract effective epsilon parameters.

Step 9: After extracting the epsilon effective parameters as shown below in Figure 3.16 for the metal fills, we can place these values in dielectric where these metal fill structures are placed and therefore remove the metal fills from the layout and hence speed up the simulation. For example, if the metals are placed in the dielectric layers from 1C to 8A, we will place the found effective epsilon parameters in these dielectric layers and remove the metal as shown in Figure 3.17.

$$\varepsilon_x - \boxed{4.4512 + 0.0003i} \qquad \mu_x - \boxed{1.0774 - 0.0055i}$$
$$\varepsilon_y - \boxed{4.4111 + 0.0004i} \qquad \mu_y - \boxed{1.0750 - 0.0054i}$$
$$\varepsilon_z - \boxed{4.1160 + 0.0046i} \qquad \mu_z \ - \boxed{1.0340 - 0.0037i}$$

Figure 3.16.: Epsilon Permittivity and Permeability

Figure 3.17.: Step 9 - Placing the epsilon effective parameters in dielectric layers

This is the entire design flow methodology which incorporates the Oblique Incidence Method. The advantage of using this design flow methodology is that the effect of metal fills can be taken into account before this goes out to the DRC check stage and therefore to the fabrication stage.

3.2.2. Comparison Of The Oblique Incidence Method When Using A 3D Numerical Tool Versus The ADL Tool

The ADL tool developed by the Terahertz Sensing group as mentioned before is built for metal fills with zero thickness which assumes the structure to be 2D. The equivalent epsilon parameters are constant with frequency when the sub wavelength metal fills are designed. When the metal fills become comparable to the wavelength at really higher frequencies, dispersive behaviour will occur.
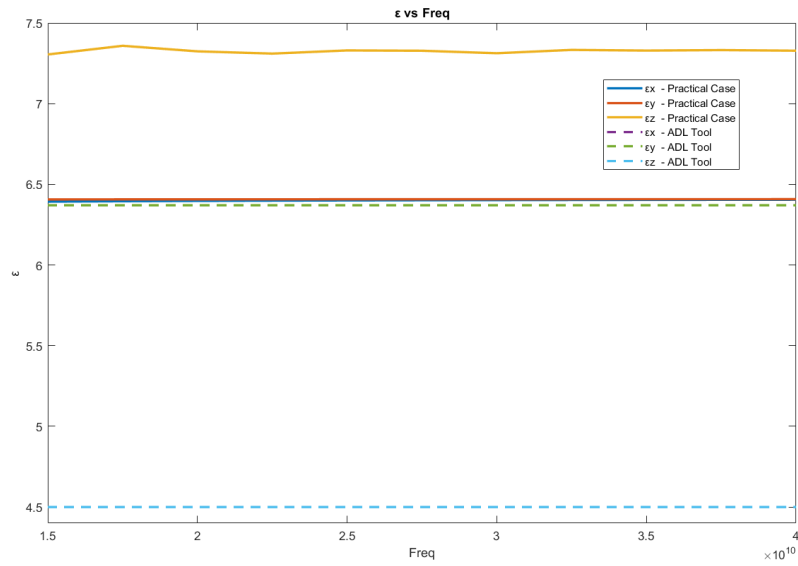
(a)
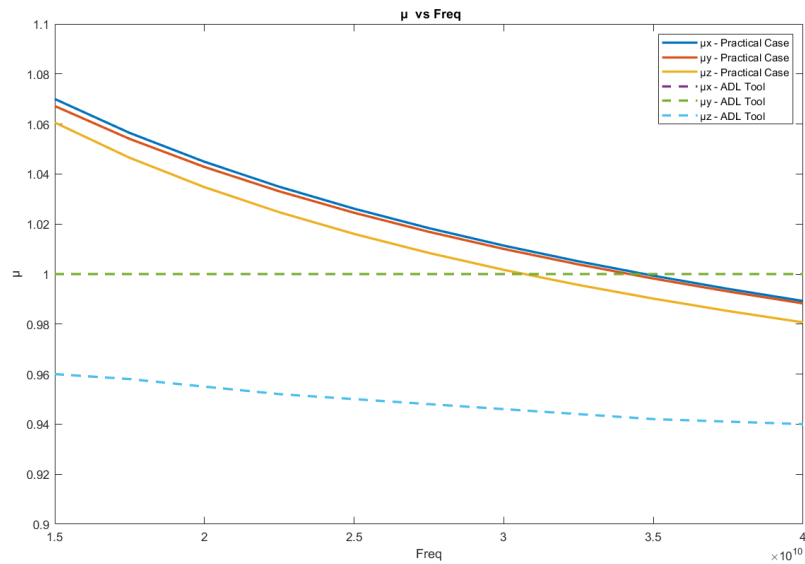
(b)

Figure 3.18.: (a) Epsilon Permittivity (b) Epsilon Permeability

It has to be noted that for the ADL case with zero thickness for the metal fill, the permittivity component ε_z remains the same value of the host dielectric because the electric field does not come in contact in the horizontal direction of the metal fill. However, in practical scenario the metal fills will have certain thickness depending on the technology that is being used in 3D EM tools. When considering the top metal layers (i.e. M7-M8) of the stack with the dimensions of the metal fills being 0.8 micron (for eg: The calculation frequency is 15-40GHz and hence it represents sub wavelength metal fills) with spacing between the metal fills is 1.47 micron and the

thickness of the metal fill is 0.79 micron which is comparable to the dimension, it is necessary to account for the offset in the z direction due to the effect of electric field that comes in contact with the metal fills with thickness in the z direction and hence the change in the permittivity component ε_z. Figure 4.6a shows the comparison of the ε and μ for i) ADL tool which considers zero thickness (dashed line) ii) Top layer metal fills (M7-M8) with thickness of 0.79 micron (solid line). It is seen that the z component of realistic case with a certain thickness of 0.79 micron (yellow solid line) shows a variation of close to 60% with the ADL case with zero thickness (light blue dashed line) because the interaction of the electric field is the z direction is high when compared to the case with the ADL tool that considers zero thickness. For the x and y component of permittivity, the change is very small which is less than 2%. For the permeability, there is a slight offset in the realistic case when compared to the ADL case with zero thickness because of the amount of current that passes through the metal fill with thickness is higher.

3.3. Scalar Number Extraction Approach

The usage of the equivalent layer found using the Oblique Incidence Method can be done quite accurately using 3D EM solvers where permittivity and permeability tensors can be employed, and is less accurate in 2.5D EM solver where only a scalar number can be provided. Due to this reason, this section will describe the extraction of scalar number using two approaches namely Electric Field Approach and Brute Average Approximation Approach by making use of equivalent layer values found from the Oblique Incidence Method and therefore utilize this scalar number in 2.5D EM tools in order to improve accuracy.

i) **Electric Field Approach -** In this approach, we can obtain a scalar number by taking the area where the field lines are running below the structure as shown below in Figure 3.19 by taking the weighted average of the horizontal and vertical components by making use of the Oblique Incidence Method (i.e. using the diagonal values of permittivity and permeability).
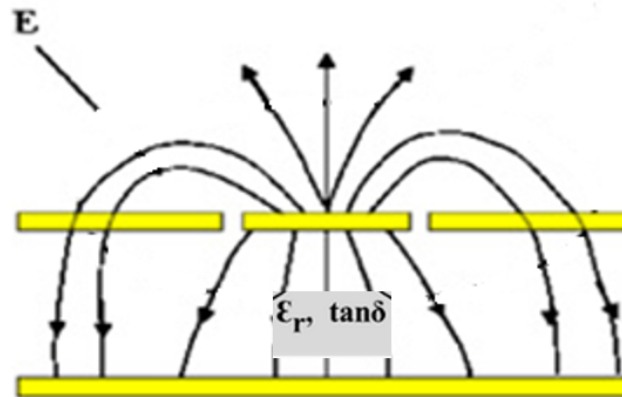
Figure 3.19.: Grounded Coplanar Waveguide

We will look into the procedure on how to extract a scalar number from the Electric Field Approach by considering a CPWG structure as shown in Figure 3.20.
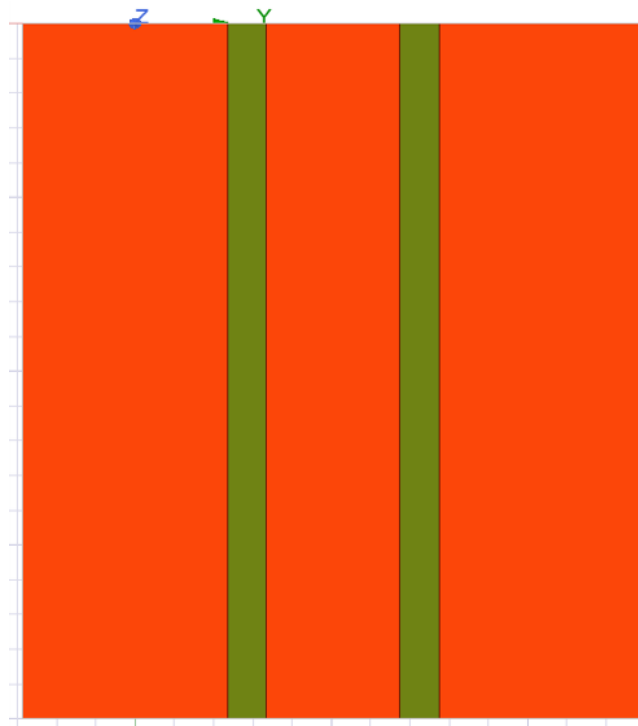
Figure 3.20.: CPWG

We are going to consider that the CPWG structure is uniform along the propagation length and hence considering the electric field only along one crosscut (i.e. YZ plane)

as shown below in Figure 3.21. This electric field data is then exported by mentioning the grid dimensions of the dielectric (square boxes) to the MATLAB script shown in Appendix which uses the below equations by taking the weighted average for the horizontal and vertical component taken from the Oblique Incidence Method (i.e. Y and Z component of the diagonal permittivity and permeability values) as shown in Figure 3.16 to find the scalar epsilon permittivity and permeability.

Summation of the electric field in the shown crosscut direction (i.e. Y and Z direction) and finding the percentage of contribution of the electric field in the horizontal direction (Y) and vertical direction (Z).

$$Percentage\ E_y = (SumE_y/Total\ sum) * 100,$$

$$Percentage\ E_z = (SumE_z/Total\ sum) * 100,$$

$$Percentage\ H_y = (SumH_y/Total\ sum) * 100, \tag{3.1}$$

$$Percentage\ H_z = (SumH_z/Total\ sum) * 100,$$

where Total sum is the total field contribution in the y and z direction.

The next step is to extract the scalar permittivity and permeability value as mentioned above from the field contribution by making use of the diagonal values found from the Oblique Incidence Method as shown in Figure 3.16.

$$Ey = 4.4111 * (Percentage\ Ey/100),$$

$$Ez = 4.1160 * (Percentage\ Ez/100),$$

$$My = 1.075 * (Percentage\ My/100), \tag{3.2}$$

$$Mz = 1.034 * (Percentage\ Mz/100),$$

By using the procedure above, we extract a scalar permittivity value of 4.1410 and permeability value of 1.0688. Hence this approach can be done for transmission line structures where the electric field is constant throughout the crossection of the line.
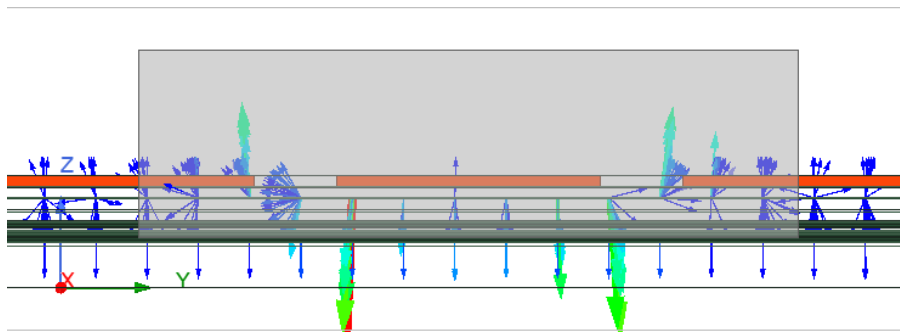
Figure 3.21.: Field contribution for CPWG

ii) **Brute Average Approximation -** This is a simple approach that can be utilized from the Oblique Incidence Method by just taking the mean of the epsilon tensor values in the vertical and horizontal direction as shown in Figure 3.16 in order to extract a scalar number. In some structures, the above mentioned Electric Field Approach cannot be implemented because the field changes across different crosscuts and hence this approach could be used where we extract a scalar number by taking mean from the Oblique Incidence Method. Since this approach directly takes the average it could lead to an error in value. So by taking the mean, we get the epsilon permittivity value of 4.26355 and epsilon permeability of 1.0545. So for this simple case, it gives a variation close to 9% for permittivity value and close to 4% for the permeability value. In Chapter 5, we will consider more specific cases where this analysis will be investigated further.

3.4. Discussion/Conclusion

In this chapter we have seen that the Unit Cell Approach using Floquet ports are used for planar periodic structures. This is suitable for structures like the metal fills where the structures are physically and electrically the same. Then the validation of the Oblique Incidence Method that makes use of the Unit Cell Approach is done for i) Homogeneous material, ii) Anisotropic material and iii) the metal fill inclusion in the dielectric. This is followed by the entire design flow methodology (steps) that incorporates the Oblique Incidence Method for the extraction of effective parameters using Unit Cell Analysis. A summary of the design flow methodology is shown below in Figure 3.22. Then the impact of the thick metal fills was seen in the z direction of permittivity component when compared to the ADL tool which considers zero thickness. Finally, two approaches namely Electric Field Approach and Brute Average Approximation Approach was discussed to extract a scalar number from the Oblique Incidence Method with improved accuracy and this scalar number can hence be used in 2.5D EM tools.

```
┌─────────────────────────────────────────────┐
│  ┌───────────────────────────────────────┐   │
│  │     Structure in 2.5D EM Tool          │   │
│  │      (Cadence Virtuoso EMX)            │   │
│  └───────────────────────────────────────┘   │
│                    │                          │
│                    ▼                          │
│  ┌───────────────────────────────────────┐   │
│  │        Generating GDS File             │   │
│  └───────────────────────────────────────┘   │
│                    │                          │
│                    ▼                          │
│  ┌───────────────────────────────────────┐   │
│  │       Generating Technol-              │   │
│  │     ogy File & Layermap File           │   │
│  └───────────────────────────────────────┘   │
│                    │                          │
│                    ▼                          │
│  ┌───────────────────────────────────────┐   │
│  │     Importing the Structure in 3D      │   │
│  │      EM Tool (HFSS 3D Layout)          │   │
│  └───────────────────────────────────────┘   │
│                    │                          │
│                    ▼                          │
│  ┌───────────────────────────────────────┐   │
│  │       Airbox Extent Definition         │   │
│  └───────────────────────────────────────┘   │
│                    │                          │
│                    ▼                          │
│  ┌───────────────────────────────────────┐   │
│  │    Export Structure to HFSS Modeller   │   │
│  └───────────────────────────────────────┘   │
│                    │                          │
│                    ▼                          │
│  ┌───────────────────────────────────────┐   │
│  │      Set up Boundary Condi-            │   │
│  │       tions and Floquet Ports          │   │
│  └───────────────────────────────────────┘   │
│  ┌───────────────────────────────────────┐   │
│  │   Embedding The Oblique Incidence      │   │
│  │  Method By Placing the Epsilon Effec-  │   │
│  │   tive Parameters in Dielectric Layers │   │
│  └───────────────────────────────────────┘   │
└─────────────────────────────────────────────┘
```

Figure 3.22.: Summary - Design Flow Methodology

4. Validation Of The Approaches Using Test Cases

In this chapter, first the validation of the Oblique Incidence Method presented in Section 3.2 for the 3D EM tool will be done for two test cases which are wave propagating structure and lumped structure namely CPWG and Stacked Transformer. This will be followed by the validation of the Scalar Number Approaches presented in Section 3.3 for the 2.5D EM tool which will be presented for the CPWG structure.

4.1. Validation Of The Oblique Incidence Approach For The 3D EM Tools Using RF Passive Structures

In this section, we will corroborate the Oblique Incidence Method as discussed in the last chapter in section Section 3.2 to consider the effect of metal fills for i) CPWG , ii) Stacked Transformer. A brief description of the two test cases will be given before moving to the implementation of the Design Flow Methodology using the Oblique Incidence Method.

i) **Grounded Coplanar Waveguide (CPWG) -** Classical CPWG is made up of a conductor separated by two ground planes, all present on the same plane on top of the dielectric medium and a ground plane is provided on the opposite side of the dielectric as well. Both digital and RF designs use on-chip transmission line structures which are crucial interconnections schemes [30]. As the metal fill density rules are getting more demanding for the smaller technological nodes as mentioned in Chapter 1, requiring the metal fill impact to be handled earlier in the implementation process for RF components. The advantage of using a CPWG structure is that it provides good field confinement in the dielectric below the line and can be simply analyzed since the EM fields is constant throughout the crossection of the line. With the ground structure present, the CPWG gives low loss performance and also gives lower radiation loss at higher frequencies [31]. For this test case, we will analyse the WCB error metric for the S Parameters.

ii) **Stacked Transformer -** The Stacked Transformer test case provided by NXP Semiconductors is a lumped structure where the wave propagation effects can be neglected. The structure is designed as two lumped coupled inductors tuned to be providing the right impedance transformation at the frequency of interest. As already mentioned above, since the metal fill density design rules for RF and digital

design system are becoming stringent for smaller nodes, it is therefore more important to consider the effects of metal fill on RF/passive components like the Stacked Transformer structure. On-chip Stacked Transformers are considered to be one of the main components in many RF applications. The main advantage of using a Stacked Transformer is that it gives better coupling factors with low area-budget and it is also fully-compatible with standard IC process technology [32]. It can be understood from the name that the Stacked Transformer layout can be realized by positioning multiple metal layers on top of each other to make three-dimensional structures which allows better coupling. Due to their increased coupling factor behavior and small area requirement, stacked on-chip transformers are becoming very popular in many applications. For this test case, we will analyse the critical Stacked Transformer parameters like the Inductance of the Primary (Lp) and Secondary coil of the Transformer(Ls), Mutual Inductance (MI), Quality Factor (Q), Coupling Coefficient (K) and Power Gain of the Transformer (PG) [33]. These critical parameters are discussed in detail in the later section.

4.1.1. Oblique Incidence Approach For the 3D EM Tools - CPWG

In this subsection, we will validate the Design Flow Methodology that makes use of the Oblique Incidence Method shown in Section 3.2 for the CPWG structure by analysing the WCB error metric for the S Parameters.

The metal layers from Metal 1 to Metal 8 (M1-M8) is used from the 28nm technology stack layer as shown in Figure 4.1. The metal fills for this test case are placed in the bottom layers from Metal 2 to Metal 6 (M2-M6) with the ground plane being placed in Metal 1 (M1). The width and the length (dimensions) of the metal fills are 0.3 micron and the spacing between the metal fills is 0.55 micron. Moreover, the inter layer dielectric height (IMD 1C-IMD 8A) is 3.005 micron and the thickness of the bottom metal fills (M2-M6) is 0.093 micron given by the technology layer stack.

The effect of the metal fills can be found by applying from **Step 1 to Step 8** as shown in Section 3.2. First, the metal fills placed in the bottom layers (M2-M6) are designed in the Cadence Virtuoso EMX which is a 2.5D EM tool and using the three important files namely GDS, technology and layermap files, the metal fills can be translated to HFSS which is a 3D EM tool. An airbox is defined for the metal fill structure with the vertical distance of the airbox being quarter wavelength and the horizontal distance given as half the spacing of the metal fill structure on each side in order to make it an unit cell which is periodic in nature. Next, the Floquet boundary conditions and Floquet ports is applied that make use of vertical (TE) and horizontal (TM) components at an oblique incidence (30 °) and normal incidence. By using this, we can extract the S Parameters at a given frequency (for this case it is chosen at 75GHz) and placing the extracted S Parameters in MATLAB script that uses Equation 2.25 to Equation 2.31 as shown in Section A.1 (Appendix), we can extract the effect of the bottom metal fills (M2-M6) as effective epsilon parameter values as shown below in Figure 4.2.

4. *Validation Of The Approaches Using Test Cases*
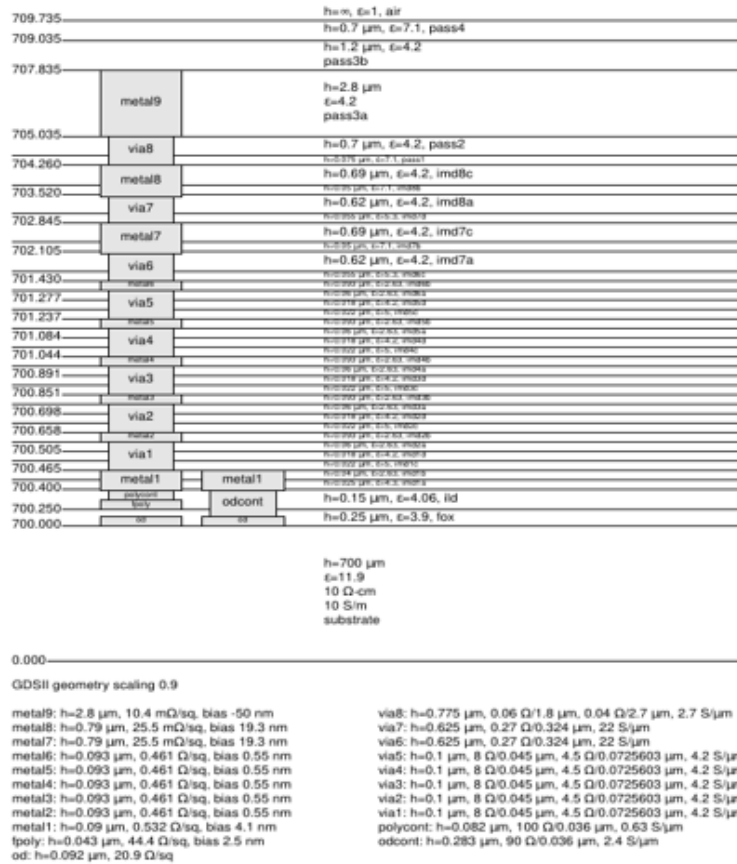
Figure 4.1.: 28nm Technology Layer Stack

$$\varepsilon_x - \boxed{4.4512 + 0.0003i} \qquad \mu_x - \boxed{1.0774 - 0.0055i}$$
$$\varepsilon_y - \boxed{4.4111 + 0.0004i} \qquad \mu_y - \boxed{1.0750 - 0.0054i}$$
$$\varepsilon_z - \boxed{4.1160 + 0.0046i} \qquad \mu_z \ - \ \boxed{1.0340 - 0.0037i}$$

Figure 4.2.: Effective epsilon parameter values using Oblique Incidence Method

Until this point we observe the effective epsilon parameters for the metal fills (M2-M6). Now the CPWG structure with metal fills (M2-M6) is designed in Cadence Virtuoso EMX (2.5D EM Tool). The designed CPWG structure is a conductor placed in between two ground conductors placed on Metal 8 (M8) on top of the dielectric layers as shown below in Figure 4.3. The dimensions of the CPWG structure is width = 16.5 micron, length = 100 micron and gap = 5 micron. By using the same steps as above, we can translate the structure to the HFSS Modeller (3D EM tool) as shown below in Figure 4.4.

Layers Used

CPWG dimensions

M1 –Ground plane [shield]
M2 to M6 – Metal fills
M8 - CPW
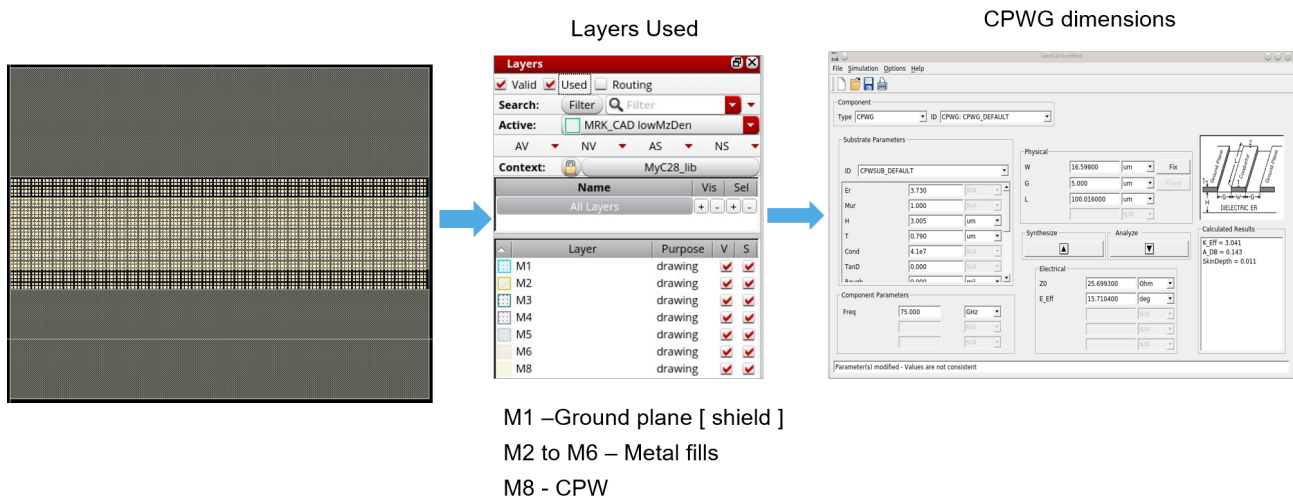
Figure 4.3.: CPWG with metal fills in Cadence Virtuoso EMX

After the CPWG structure with metal fills (M2-M6) is placed in HFSS Modeller as shown in Figure 4.4 , the first step is to simulate the CPWG case with all the metal fills and have it as the reference case. The subsequent step is to simulate the CPWG case by removing the metal fills by having the same nominal layer stack values for the dielectric layers (i.e. not making any changes in the dielectric values).
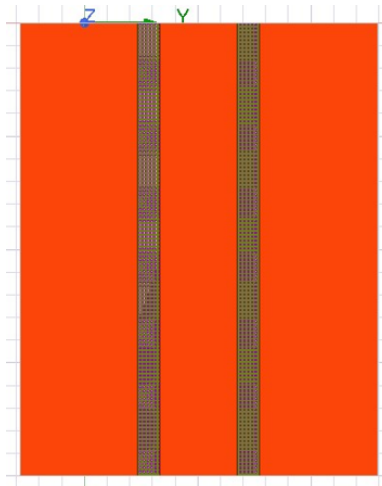
Figure 4.4.: CPWG structure with metal fills in HFSS Modeller

The next step is to introduce the found effective epsilon parameters as found in Figure 4.2 in the dielectric layers (i.e IMD 1C-IMD 8C) and remove the metal fills from the CPWG structure as shown in Figure 4.5.
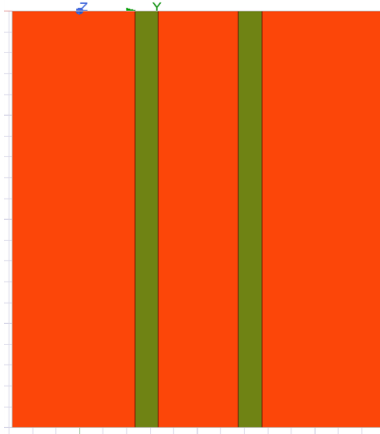
Figure 4.5.: CPWG structure without metal fills in HFSS Modeller

In order to compare the performances of the CPWG case for i) removing the metal fills by having the same dielectric values (i.e. nominal layer values) and ii) using the Oblique Incidence Method in order to take into account the effect of metal fills as complex epsilon parameter values, we consider the case with metal fills as the reference. Then, by defining an error metric for S Parameters [34] as shown below,

$$WCB = max|\overline{S_{ij}} - S_{ij}| \tag{4.1}$$

where, $\overline{S_{ij}}$ is the reference S Parameters for the case with metal fills and S_{ij} is the S Parameters resulting from the case with no metal fills by taking the same nominal layer stack values and the Oblique Incidence Method. i,j represent [1,2] . Figure 4.6 represents the S11 comparison and the S21 comparison between the case with metal fills, the Oblique Incidence Method and the no fill having the same nominal layer stack. Figure 4.7 shows the results of the error metric vs frequency for both the case with no fills (dark blue circle) and the case with Oblique Incidence Method (red circle). The plot shows that a lower error value is seen for the case with the Oblique Incidence Method when compared to the case with no metal fills using the nominal layer stack values. However, if we have to simulate the CPWG structure with all the metal fills, the simulation time drastically increases (close to 2 days). The use of the Oblique Incidence Method which takes into account the effect of metal fills as complex effective parameter values gives the result with good accuracy and reduced simulation time (less than 10 minutes).
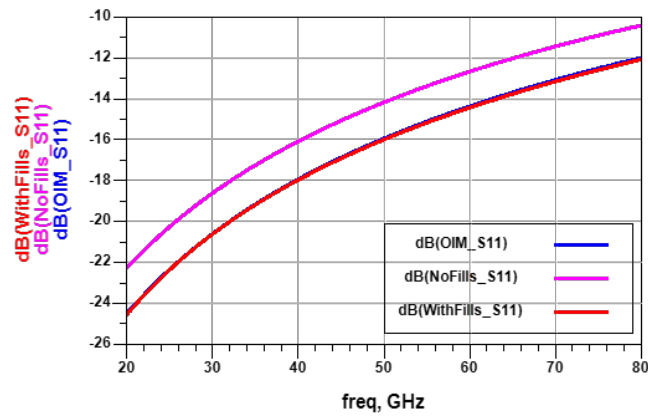
(a)
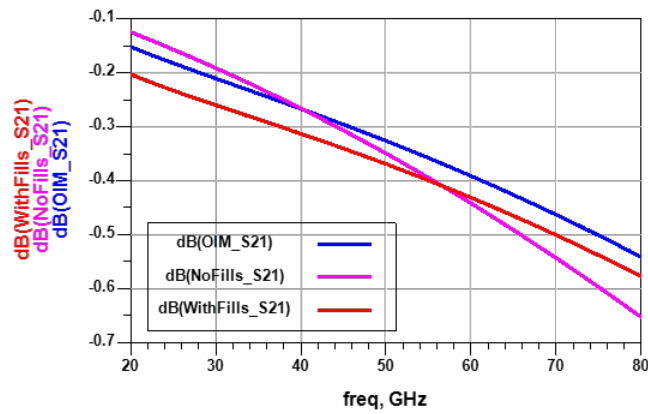
(b)

Figure 4.6.: (a) S11 (b) S21
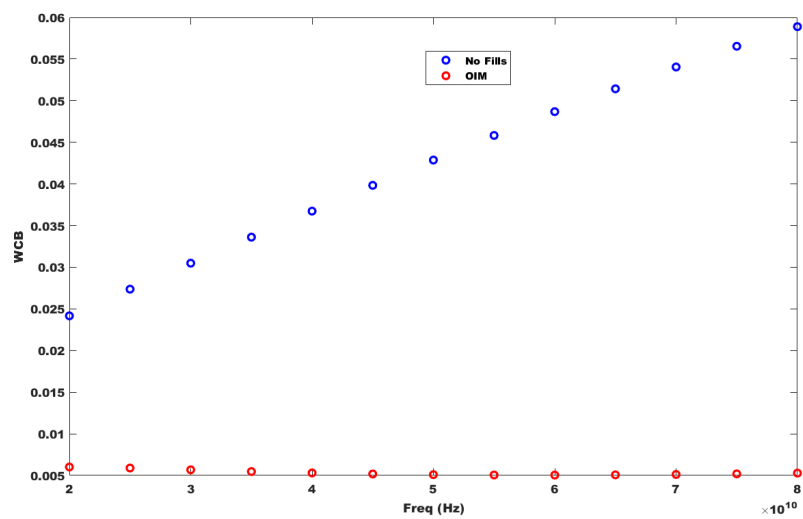
Figure 4.7.: WCB - No Metal Fills (i.e. Considering same layer stack values) and Oblique Incidence Method

4.1.2. Oblique Incidence Approach For The 3D EM tools - Stacked Transformer

The same 28nm technology stack layer shown in Figure 4.1 is used. For this test case provided by NXP Semiconductors, the metal fills placed in the top layers (M7-M8) are analysed and the bottom layer metal fills (M2-M6) were ignored due to two reasons, i) the primary reason being that there was no measurement data to compare the results and ii) the simulation time and the memory usage will be really high due to placement of lot of bottom layer metal fills (M2-M6).

Now focusing on the details of the metal fills (M7-M8), the width and the length (dimensions) of the metal fills are 0.8 microns and the spacing between the metal fills is 1.58 micron. The inter layer dielectric height is 1.58 micron (IMD 7B-IMD 8C) and the thickness of the top metal fills (M7-M8) is 0.79 micron.

Like the CPWG case, the effect of the top metal fills (M7-M8) can be found by applying from **Step 1 to Step 8** as seen in section 3.2. The metal fills placed in the top layers (M7-M8) is designed in Cadence Virtuoso EMX and translated to HFSS Modeller by using the GDS, technology and layermap files. Airbox is defined for the metal fill structure with vertical padding being quarter wavelength and the horizontal padding is given as half the spacing of the structure on each side in order to make it an unit cell which is periodic in nature. The Floquet boundary condition and Floquet ports is applied under two angle of incidences which are the normal and oblique incidence for two types of excitation (i.e. TE and TM) for which the S Parameters can be extracted. The effect of metal fills was seen at 3 different frequencies (5GHz, 20GHz and 40GHz) for this test case. The S Parameters is then exported to the MATLAB script to obtain the effective epsilon parameter values for the top metal fills (M7-M8) as shown below in Figure 4.8

So, after extracting effective epsilon parameters for the top layer metal fills (M7-M8), the next step is to translate the Stacked Transformer test case provided by NXP Semiconductors from Cadence Virtuoso EMX to HFSS Modeller by following the same procedure as before as shown below in Figure 4.9 and Figure 4.10. The Stacked Transformer structure has its primary coil placed on Metal 8 (M8) and secondary coil along with the center tap placed on Metal (M7) and also from this detail we can understand that the metal fills are placed on the same layers as the functional layer (i.e. primary and secondary).

After translating the Stacked Transformer structure with the top metal fills (M7-M8) to HFSS Modeller, the first step is to simulate the Stacked Transformer with all the metal fills and use it as a reference case. This will be subsequently followed by removing the metal fills from the structure by having the same values as the layer stack for the dielectric layers. The next step is to place the found effective epsilon parameters at three different frequencies (5GHz, 20GHz and 40GHz) as shown in Figure 4.8 in the dielectric layers (i.e. IMD 7B- IMD 8C) and remove the top metal fills from the Stacked Transformer structure as shown in Figure 4.11

$\varepsilon_x -$ | 6.3745 - 0.0022i

$\varepsilon_y -$ | 6.4041 - 0.0003i

$\varepsilon_z -$ | 7.2184 - 0.0016i

$\mu_x -$ | 1.1328 - 0.1302i

$\mu_y -$ | 1.1270 - 0.1299i

$\mu_z -$ | 1.1299 - 0.1522i

(a)

$\varepsilon_x -$ | 6.3761 - 0.0022i

$\varepsilon_y -$ | 6.4075 - 0.0001i

$\varepsilon_z -$ | 7.2583 - 0.0032i

$\mu_x -$ | 1.0445 - 0.1238i

$\mu_y -$ | 1.0394 - 0.1235i

$\mu_z -$ | 1.0347 - 0.1297i

(b)

$\varepsilon_x -$ | 6.3779 - 0.0020i

$\varepsilon_y -$ | 6.4045 - 0.0003i

$\varepsilon_z -$ | 7.3224 - 0.0072i

$\mu_x -$ | 0.9887 - 0.1107i

$\mu_y -$ | 0.9842 - 0.1104i

μ_z | 0.9807 - 0.1088i

(c)

Figure 4.8.: (a) Effect of metal fills at 5GHz (b) Effect of metal fills at 20GHz (c) Effect of metal fills at 40GHz

Test Case – Stacked Transformer

Layers Used

M1 –Ground plane

M7 – CT & Secondary

M8 – Primary
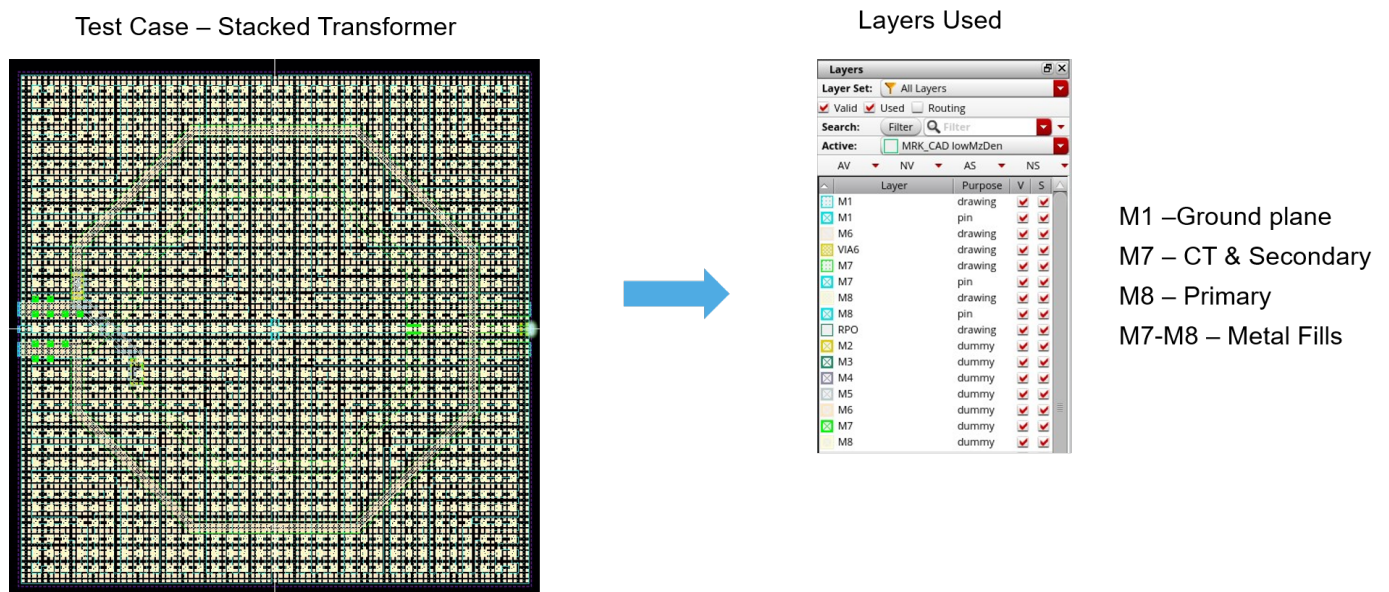
M7-M8 – Metal Fills

Figure 4.9.: Stacked Transformer with metal fills in Cadence Virtuoso EMX
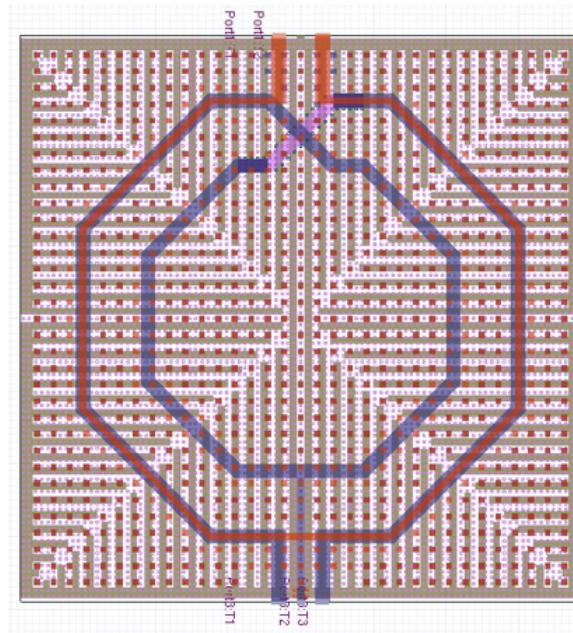
Figure 4.10.: Stacked Transformer with metal fills in HFSS Modeller
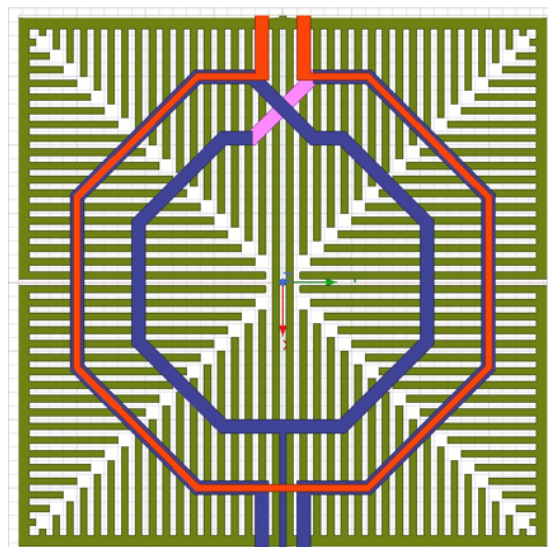
Figure 4.11.: Stacked Transformer without metal fills in HFSS Modeller

The following step is to emphasize on the performance of the Stacked Transformer by focusing on the critical parameters which are the Inductance of the Primary (Lp) and Secondary coil (Ls), Mutual Inductance (MI), Quality Factor (Q), Coupling Coefficient (K) and Power Gain (PG) of the Transformer [32] [33] for all the cases mentioned above. These parameters are analysed by converting S Parameters to Z and Y parameters. Before we examine, a brief description of the parameters is given.

i) Primary Inductance (Lp), Secondary Inductance (Ls) and Mutual Inductance (MI): A Stacked Transformer can also be seen as two inductors coupled together.

Inductance is the property of the inductor that tends to oppose any change in the current flow (both primary and secondary). Mutual Inductance occurs when the change in current in one inductor induces a voltage in another inductor. It is important to consider these parameters since this is the mechanism by which transformers work. The equation of Primary, Secondary and Mutual Inductance is represented as follows:

$$Lp = Imag(Z_{11})/2\pi f \tag{4.2}$$

$$Ls = Imag(Z_{22})/2\pi f \tag{4.3}$$

$$MI = Imag(Z_{12})/2\pi f \tag{4.4}$$

where

Lp- Primary Inductance,

Ls- Secondary Inductance,

MI- Mutual Inductance,

f - frequency

ii) Quality Factor (Q): Quality Factor is defined as the ratio of energy stored in coil to the energy dissipated by the coil and it provides an indication of the losses and how efficient the transformer is and therefore it plays a key role. Hence, the main goal for the designers is to maximize the Q factor. A simple equation for the Q Factor is given as:

$$Q = -Imag(Y_{11})/Real(Y_{11}) \tag{4.5}$$

iii) Coupling Coefficient (K): Coupling Coefficient is defined as the magnetic coupling between the primary and secondary coils of the transformer. As mentioned before, generally the stacked transformer gives a larger coupling coefficient due to its metal layers being closely packed with each other and hence there would be overlapping. Generally, the Coupling Coefficient is stated as:

$$K = \frac{MI}{\sqrt{(LpLs)}} \tag{4.6}$$

iv) Power Gain (PG): Power gain is defined as the ratio of output power to the input power. In realistic scenarios, there would be losses which would decrease the output power from the input power and therefore this parameter is critical.

$$PG = 1 + 2(x - \sqrt{x^2 - x}) \tag{4.7}$$

where,

$$x = \frac{Real(Z_{11})Real(Z_{22}) - |Real(Z_{12})^2}{|Imag(Z_{12})|^2 + |Real(Z_{12})|^2} \tag{4.8}$$

Figure 4.12 shows the analyses of the critical Stacked Transformer parameters vs frequency using the above equations for the cases i) with all the metal fills present

53

in the Stacked Transformer (red colour curve), ii) removing the metal fills by having the nominal layer values (dark blue colour curve), iii) using the Oblique Incidence Method at three different frequencies (5GHz- pink colour curve, 20GHz - light green colour curve and 40GHz - black colour curve) to take into account the effect of metal fills as complex effective parameters. Both the cases, with metal fills and without metal fills are represented by solid curve and the Oblique Incidence Method is represented by dashed curve. The plot shows that the case with no metal fill having the nominal layer values shows a fair amount of deviation with the metal fill case (reference) and the variation becomes more prominent as the frequency increases for all the parameters except Quality factor and Power Gain where the deviations are minimal. So, it is important to consider the effect of metal fills but practically it is not possible to simulate the structure due to the increased simulation time (close to 4 hours). Therefore it is seen from the plot that the Oblique Incidence Method (dashed line) shows good matching with the metal fill case (reference) with reduced simulation time (less than 10 minutes). We can also understand from the plot that the effect of metal fills evaluated using Oblique Incidence Method does not vary with frequency (i.e. frequency independent) and hence the plot at different frequencies almost overlap each other.

4.2. Validation Of The Scalar Number Approach For 2.5D EM Tools

As mentioned in the last chapter in Section 3.3, the scalar number extraction can be done using Electric Field Approach and Brute Average Approximation Approach. The Electric Field Approach is based on taking the weighted average of the horizontal and vertical component of tensor behavior by making use of the tensor values of the Oblique Incidence Method and hence this scalar number can be used for 2.5D EM tool with good precision and accuracy. The Brute Average Approximation Approach is based on taking the mean of the tensor values of the Oblique Incidence Method. By applying the procedure from the last Section 3.3 we can extract a scalar number for the CPWG structure.

First, taking into account the field under the CPWG structure and exporting the data by mentioning the grid dimensions of the dielectric (IMD 1C-IMD 8A) to MATLAB script as shown in Figure 4.13 where the weighted average for the horizontal and vertical component taken from the Oblique Incidence Method is considered as mentioned before, we get the scalar permittivity to be 4.141 and scalar permeability as 1.0688. The Brute Average Approximation Approach is performed by taking the mean of the horizontal and vertical components and we get the scalar permittivity to be 4.26355 and scalar permeability as 1.0545.

In order to compare the performances of the CPWG case for the scalar number extraction, we use the WCB error metric for the S Parameters as mentioned in the last section for i) Oblique Incidence Method ii) Electric Field Approach and iii) Brute

Figure 4.12.: (a) Lp vs Freq. (b) Ls vs Freq. (c) MI vs Freq (d) Q vs Freq. (e) K vs Freq. (f) PG vs Freq

Average Approximation and iv) No Fills having the same nominal layer value by having the case with metal fills as the reference. Figure 4.14 shows the results of the error metric vs frequency for the three cases with Oblique Incidence Method (red circle), Electric Field Approach (dark blue circle), the Brute Average Approximation

4. Validation Of The Approaches Using Test Cases

Field In 3D EM Tool   Imported Field In MATLAB
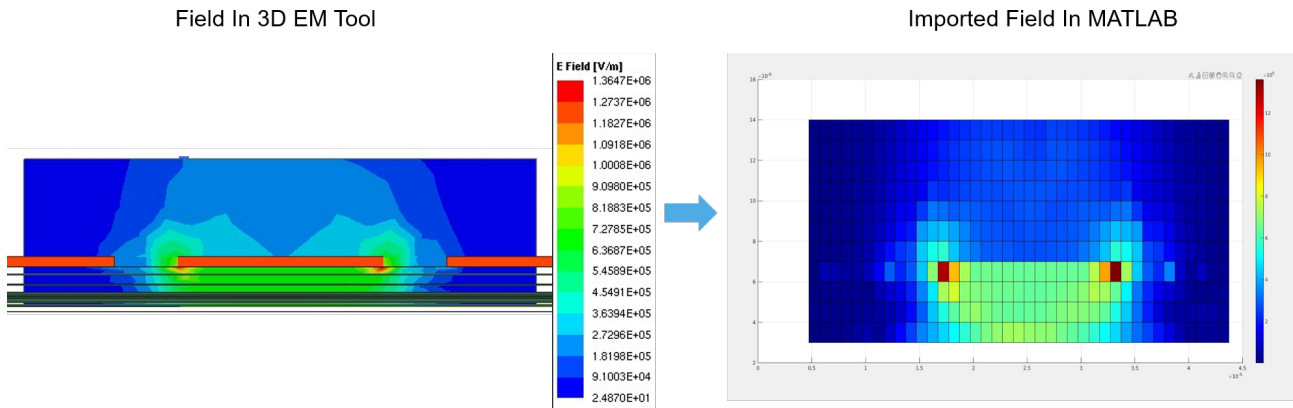
Figure 4.13.: Field in 3D EM tool and imported field in MATLAB

(pink circle) and No Fills having the same nominal layer value (light green circle). We can understand from the plot that the Brute Average Approximation Approach error metric increases when compared to the Electric Field Approach and the error increases almost twice as the frequency increases. Hence, this exhibits that the scalar number extracted from the Electric Field Approach gives a more accurate value due to the presence of the field contribution in the horizontal and vertical component by applying the weighted average and therefore this gives more knowledge and insight on the epsilon values. This could be used in the 2.5D EM tool for the transmission line structures since the extraction of the field for these structures can be done easily.
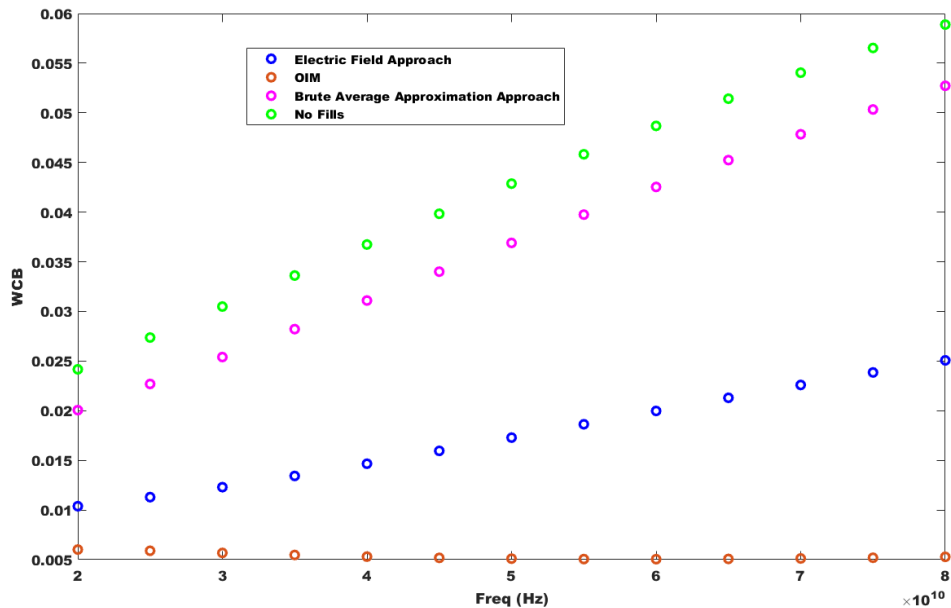
Figure 4.14.: WCB - Oblique Incidence Method, Electric Field Approach and Brute Average Approximation Approach

4.3. Discussion/Conclusion

In this chapter, we have seen the validation of the Oblique Incidence Method for the 3D EM tool performed for the two test cases namely CPWG and Stacked Transformer. For the CPWG structure, the effect of bottom layer metal fills was taken into account at 75GHz. To compare the performances of the CPWG case, WCB error metric was taken into account for i) removing the metal fills by having the same dielectric values (i.e. nominal layer values) and ii) using the Oblique Incidence Method in order to take into account the effect of metal fills as complex epsilon parameter values having the case with metal fills as the reference. A lower error value is seen for the case with the Oblique Incidence Method when compared to the case with no metal fills and it is not possible to simulate the structure with all the metal fills due to increased simulation time (close to 2 days). Hence the Oblique Incidence Method which takes into account the effect of metal fills as complex effective parameter values gives the result with good accuracy and reduced simulation time (less than 10 minutes). For the Stacked Transformer structure provided by NXP Semiconductors, the effect of top layer metal fills was taken into account at 5GHz, 20GHz and 40GHz. To compare the performances of the Stacked Transformer structure, critical parameters like Primary Inductance (Lp), Secondary Inductance (Ls) and Mutual Inductance (MI), Quality Factor (Q), Coupling Coefficient (K) and Power Gain of the Transformer (PG) was taken into account. Similar to the CPWG structure, the case with no metal fill having the nominal layer values shows a fair amount of deviation with the reference metal fill case and the variation becomes more prominent as the frequency increases. Like the CPWG structure, the case with all the metal fills increases the simulation time (close to 4 hours) and hence the Oblique Incidence Method which gives good accuracy with the metal fill case, also reduces simulation time (less than 10 minutes). It is also understood that the Oblique Incidence Method does not vary with frequency (i.e. at 5GHz, 20GHz and 40GHz curves almost overlap) and this implies that the effect of metal fills can be found at different frequencies and the impact of the change in frequency is less. Next, the validation of the Scalar Number Approach namely Electric Field Approach and Brute Average Approximation Approach for the 2.5D EM tool is performed for the CPWG structure. For the Electric Field Approach, we take into account the weighted average for the horizontal and vertical component taken from the Oblique Incidence Method and for the Brute Average Approximation Approach we take the mean of the horizontal and vertical component from the Oblique Incidence Method. The WCB error metric for the S Parameters was taken into account for i) Oblique Incidence Method, ii) Electric Field Approach, iii)Brute Average Approximation and iv) No Fills having the same nominal layer value by having the Metal Fill case as the reference. It was seen that the error from the Electric field Approach was less than that of the Brute Average Approximation Approach due to the presence of the field contribution in the horizontal and vertical component and then applying the weighted average and this scalar number could enable 2.5D EM simulation for the transmission line structures since the electric field for these structures can be extracted easily.

5. Design Based Approach

This chapter presents the insights of designing the metal fills with different shapes and alignment by implementing the Oblique Incidence Method. This is done in order to understand the variations in epsilon effective parameters. It is performed because for less epsilon variations, an accurate scalar number value can be extracted using the two approaches mentioned in Section 3.3 to enable 2.5D EM simulations with improved accuracy. We will then classify the metal fill shapes as Worst Case, Intermediate Case and Best Case scenarios based on the variation in epsilon effective parameters. This will be followed by validating this approach for the CPWG structure using the WCB error metric for the Scalar Number Extraction Approaches namely Electric Field Approach and Brute Average Approximation Approach by having the three cases (i.e. Worst Case, Intermediate Case and Best Case) found using the Oblique Incidence Method as a reference.

5.1. Analysis On Different Metal Fills

In this section we will understand the impact of different metal fills based on their epsilon variations. So, if we don't do any changes to the metal filling and just rely on the metal filling script (i.e. DRC script) which is done before the chip is fabricated, the layout density distribution increases. Generally, the Rectangle metal fill shape is used by the script which is the traditional metal fill design and most widely used. But in some cases, if there is a misalignment in the Rectangle metal fills there would be a bigger variation impact in the epsilon values [35] [26]. Hence, in order to reduce the variations of the epsilon values we can make use of two approaches, i) Align the Rectangle metal fill shape and ii) Design an optimal shape and see if we can further reduce the epsilon variation. We have to note that the same fill density should be used for the metal fills. Hence, for less epsilon variations, we can make a better approximation of the scalar number in order to enable to 2.5D EM simulations with less error and the scalar number extraction can be done using the two methods as mentioned in Section 3.3.

5.1.1. Rectangle Metal Fills

Most technology processes use the Rectangle metal fills in their implementation as mentioned before. In this analysis, we are going to analyse the bottom layer metal

fill (M2-M6) with the width and length = 0.3micron (dimension) and spacing = 0.55micron. The metal fill density is calculated as the ratio of the Metal Area to the Total Area in percentage (Metal Area/Total Area)x100. The metal fill density taken into account for this case is 12.45%. We will incorporate the Oblique Incidence Method by using the same procedure mentioned in Section 3.2.1 in order to take into account the epsilon effective parameters.

We will first start the analysis by not aligning the Rectangle metal fills as mentioned above, since this will have the maximum impact in the epsilon variation (i.e. difference between permittivity and permeability values in x, y and z direction will be high) . Figure 5.1 shows the Rectangle Misaligned metal fills.

Rectangle Misaligned Metal Fills
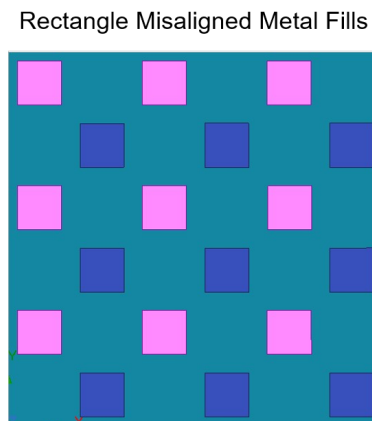
Figure 5.1.: Rectangle Misaligned metal fills

We can clearly understand from Figure 5.2 that Rectangle Misaligned metal fills shows high variation (variation between x, y and z direction) in the epsilon values (i.e. the variation for the permittivity is about 22.5% and the variation for the permeability is about 8%). This is due to the fact that the permittivity components ε_x and ε_y increase with the misalignment because of the raised mutual capacitance between layers and the variation can be seen with respect to ε_z.

(a)

(b)
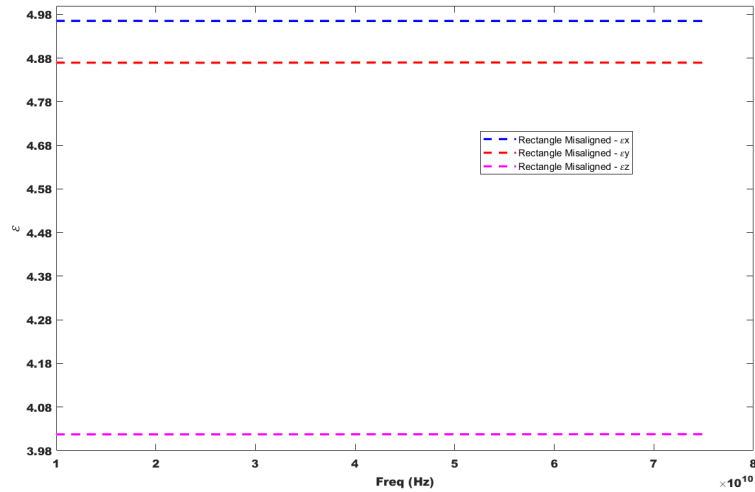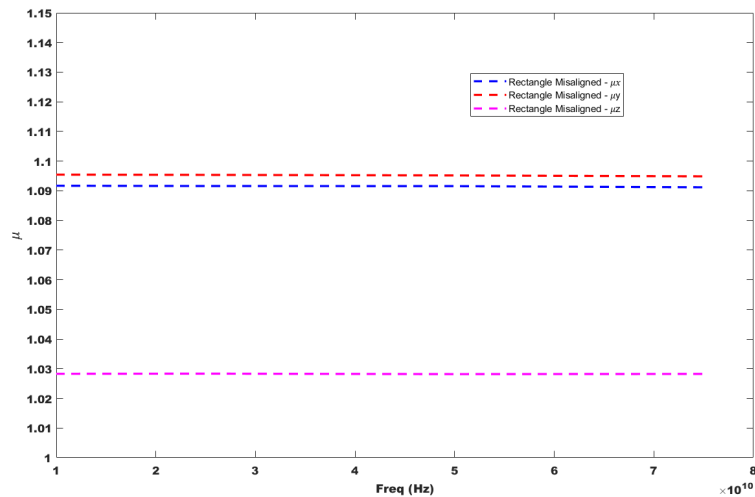
Figure 5.2.: (a) ε for Rectangle Misaligned metal fill (b) μ for Rectangle Misaligned metal fill

One way to tackle this high variation in epsilon parameter is to align the Rectangle metal fills with the same metal fill density as shown in Figure 5.3.

It can be seen in Figure 5.4 that after aligning the Rectangle metal fills, the impact of the epsilon variation has decreased (i.e. the variation for the permittivity is close to 9.3% and the variation for the permeability is around 4%). It is therefore seen that the aligned case variation for the epsilon values (i.e. the difference between in the x, y and z direction) is less than the misaligned case for the Rectangle metal fills.
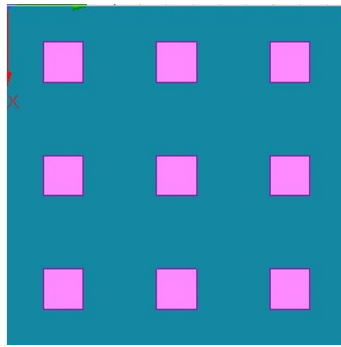
Figure 5.3.: Rectangle Aligned metal fills
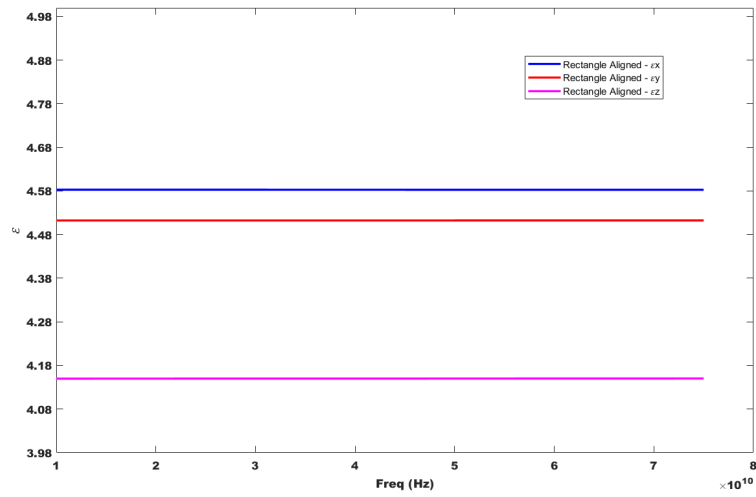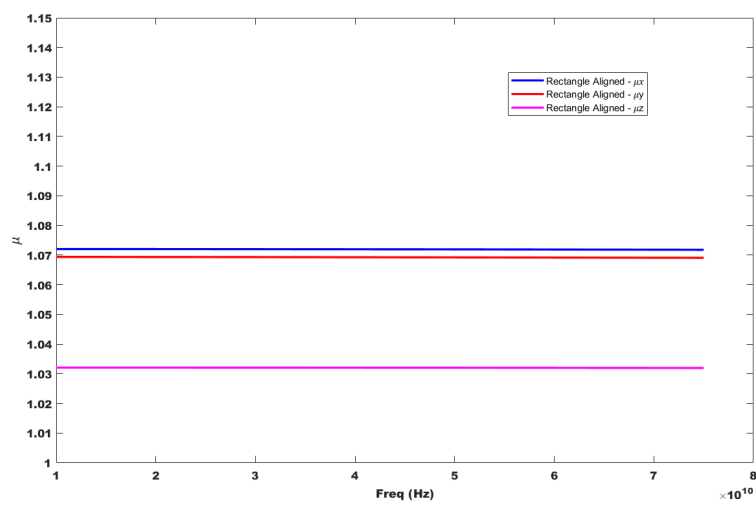
(a)

(b)

Figure 5.4.: (a) ε for Rectangle Aligned metal fill (b) μ for Rectangle Aligned metal fill

Hence this is one approach to reduce the epsilon variation by aligning the metal fills and therefore the extraction of a scalar number for 2.5D EM tools can be done with less error.

We can further see in the next subsection that by designing optimum metal fill shapes, if the epsilon variation impact further reduces or not.

5.1.2. Optimum Metal Fill Shapes

In this thesis work, we have considered two metal fill shapes which is Plus [36] and Hexagon Donut with the same metal fill density of 12.45% as the Rectangle metal fill to understand if the capacitance between layers reduces and also to see if the variation further decreases than the aligned Rectangle metal fill shape. Both the metal fills have been designed with alignment and misalignment cases as shown below in Figure 5.5 and Figure 5.6 with an eye towards the epsilon variation and to see if it further reduces.
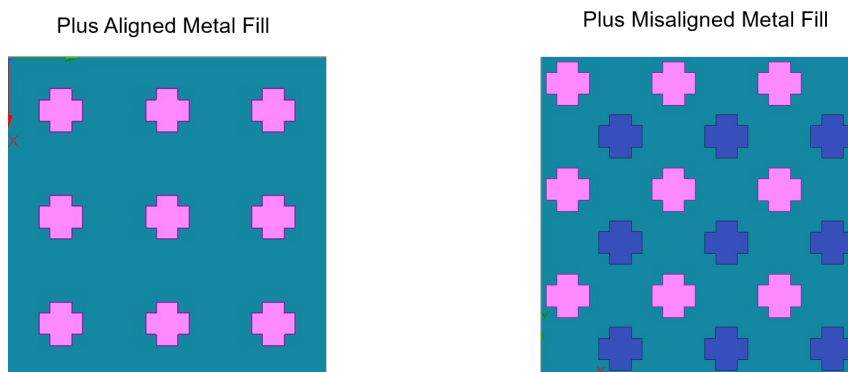
Figure 5.5.: Plus metal fills - Aligned and Misaligned
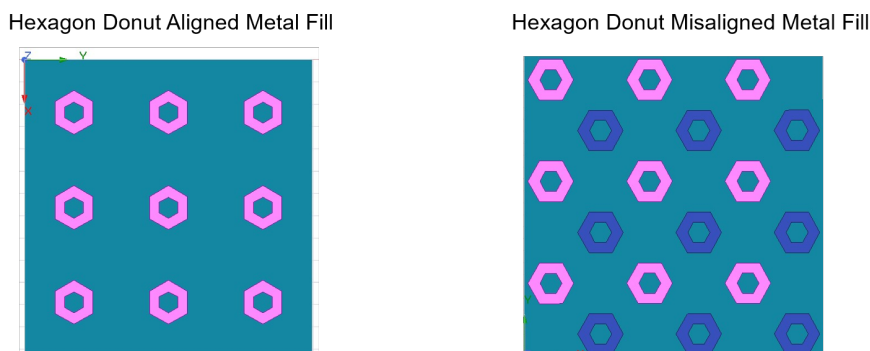
Figure 5.6.: Hexagon Donut metal fills - Aligned and Misaligned

Figure 5.7 shows that the Plus Aligned metal fill shape seems to have the least epsilon variation (i.e. the variation for the permittivity is close to 6.5% and the variation for the permeability is about 3.84%) which is followed by Hexagon Donut Aligned metal fill shape (i.e. the variation for the permittivity is close to 7.8% and the variation for the permeability is around 4%) and this shows that mutual capacitance between the layers further reduces than the Rectangle metal fills and hence we can see that the variation in ε_x and ε_y is less in both the cases with respect to ε_z. It is also understood from the plot that the misaligned metal fill shapes (represented by dashed lines) in general seems to have a greater variation than the aligned metal fill shapes (represented by solid lines) and the highest being that of the Rectangle Misaligned metal fills.

Therefore to briefly summarize, we understand that the Rectangle Misaligned metal fill shape has bigger variation in epsilon values vs frequency because the permittivity components ε_x and ε_y increase with the misalignment, because of the raised mutual capacitance between layers with respect to ε_z. In order to reduce the epsilon variation impact, two approaches were used: i) Aligning the Rectangle metal fill shape where we already see a reduction in epsilon variation. ii) Designing optimal metal fill shapes (i.e. Plus and Hexagon Donut), which further reduces the epsilon variation.

Hence for less epsilon variations, we can make a better approximation for the scalar number in order to enable to 2.5D EM simulations with less error.

In the next section, we will validate the Design Based Approach for the scalar number extraction by making use of three cases based on the alignment and optimal metal fill shape with respect to the epsilon variations for the CPWG structure. The three cases are mentioned below:

i) Worst Case : Rectangle Misaligned metal fill

ii) Intermediate Case : Rectangle Aligned metal fill

iii) Best Case: Plus Aligned metal fill

5.2. Validation Of The Design Based Approach For The Scalar Number Extraction

In this section, we will validate the Design Based Approach by using the three cases as mentioned above (i.e. i) Worst Case : Rectangle Misaligned metal fill, ii) Intermediate Case : Rectangle Aligned metal fill, iii) Best Case: Plus Aligned metal fill) for the CPWG structure by using the found epsilon values from the Oblique Incidence Method and having this as a reference case for the two scalar number approaches namely i) Electric Field Approach and ii) Brute Average Approximation Approach. This will be followed by the comparison of S Parameters results for the scalar number approaches using the WCB error metric for the three cases.
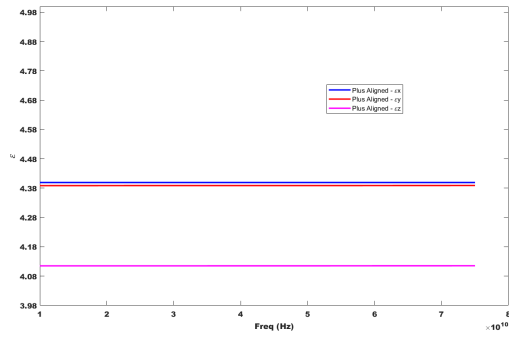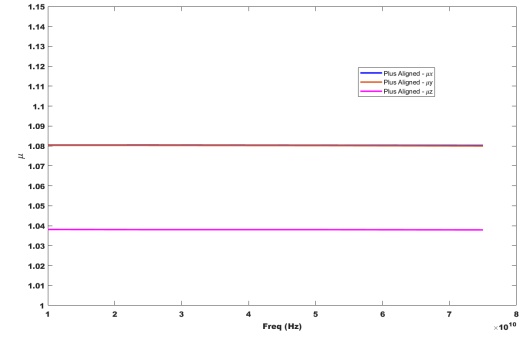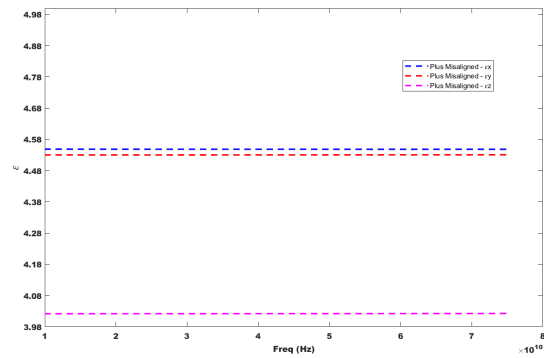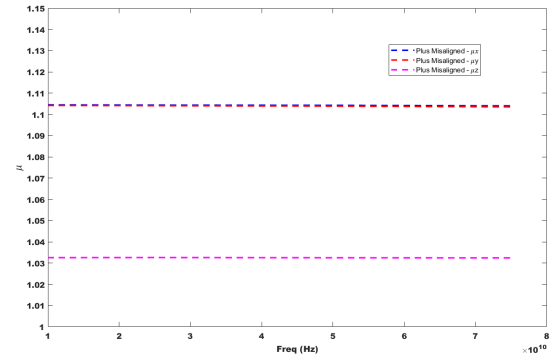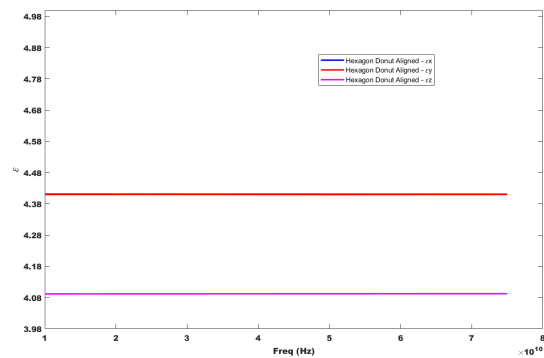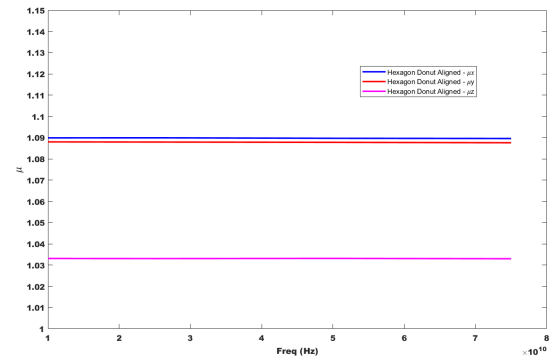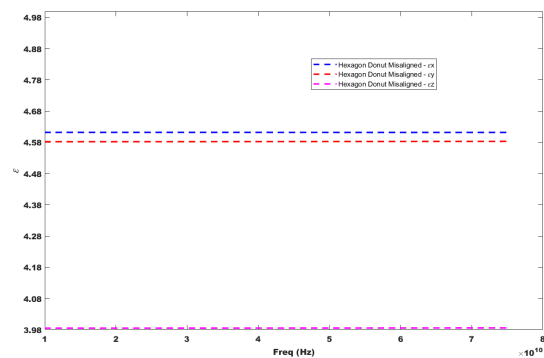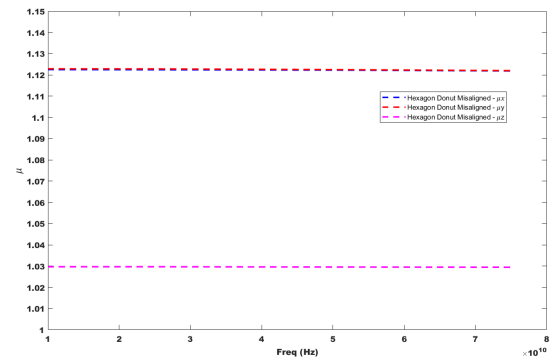
5. Design Based Approach

Figure 5.7.: (a)-(b) represents the ε and μ for Plus Aligned metal fill, (c)-(d) represents the ε and μ for Plus Misaligned metal fill, (e)-(f) represents the ε and μ for Hexagon Donut Aligned metal fill, (g)-(h) represents the ε and μ for Hexagon Donut Misaligned metal fill.

5.2.1. Scalar Number Approaches for the Three Cases

We will first make use of the epsilon values found in the last section using Oblique Incidence Method and have it as a reference case for the three cases. The Scalar Number Approaches mentioned in Section 3.3 uses the information of effective epsilon values from the Oblique Incidence Method. The Electric Field Approach takes into account the weighted average of the horizontal and vertical components running across the structure and the Brute Average Approximation Approach is done by taking the mean of the epsilon values. We will implement these approaches for the three cases.

But before implementing the scalar approach, we have to export the CPWG structure from the Cadence Virtuoso EMX which is a 2.5D EM tool to HFSS which is a 3D EM tool by following the same procedure shown in Section 3.2.1 as shown below in Figure 5.8 After translating the structure to HFSS, the first step is to place the found effective epsilon parameters values using the Oblique Incidence Method in the last section and simulate the CPWG structure for the three cases and use it as a reference case. The next step is to extract a scalar number by making make use of the Electric Field Approach mentioned in Section 3.3 by exporting the field data to the MATLAB script that makes use of the weighted average of the horizontal and vertical component found from the Oblique Incidence Method and implement the obtained scalar number and simulate for all the three cases. Finally, the scalar number using Brute Average Approximation Approach is extracted by taking the average of the epsilon values and this number is applied and simulated for the three cases.
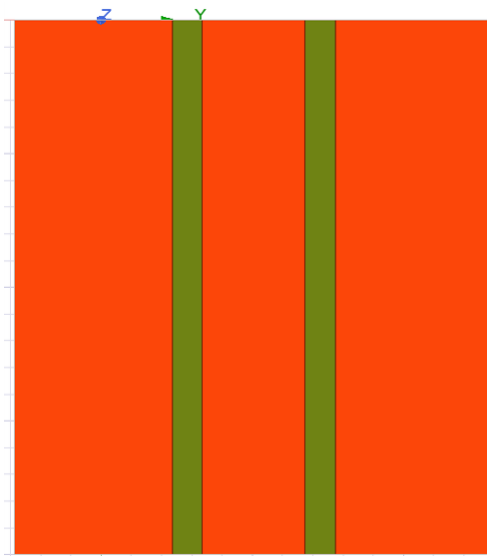
Figure 5.8.: CPWG

5. Design Based Approach

To compare the performances of the CPWG case for the three cases i) Worst Case : Rectangle Misaligned metal fill, ii) Intermediate Case : Rectangle Aligned metal fill and iii) Best Case: Plus Aligned metal fill, the WCB error metric for S Parameters will be used as done in the last chapter. $\overline{S_{ij}}$ is the reference S Parameters for the case with the Oblique Incidence Method and S_{ij} is the S Parameters resulting from the scalar number Electric Field Approach and Brute Average Approximation Approach. Figure 5.9 shows the results of the error metric vs frequency for the scalar number approaches by making use of the three cases. The circle curves represents the Electric Field Approach and the star curves represents Brute Average Approximation Approach. The Worst Case : Rectangle Misaligned metal fill is represented by red colour, Intermediate Case : Rectangle Aligned metal fill is shown by dark blue colour and Best Case: Plus Aligned metal fill is depicted as pink colour. The plot shows that least error value is seen for the Electric Field Approach extracted for the Best Case: Plus Aligned metal fill and highest error is seen in the Brute Average Approximation Approach for the Worst Case : Rectangle Misaligned metal fill. This is because taking into account the effect of field in particular direction (i.e. horizontal and vertical) gives more knowledge and insight on the epsilon variation and also it worked best for the Plus Aligned shape because the epsilon variation is the least and hence extracting the scalar number gave less error. The Electric Field Approach will work perfectly for Transmission Line structures (i.e. wave propagating structure) as extracting the electric field can be done at every cross-section of the line where the field behavior is constant except at the edges and hence the error is less, but if we move to structures like Transformers and Inductors (i.e. lumped structure) extracting the field can be really complicated and hence it is good to arrive at a solution that has metal fills with less epsilon variation (i.e. in this case, Plus Aligned metal fills) and therefore even use the Brute Average Approximation Approach where the error is less.
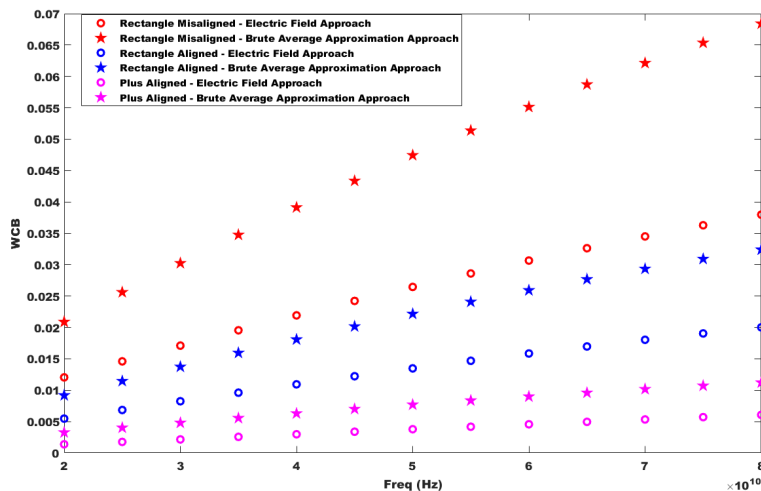
Figure 5.9.: WCB - Electric Field Approach and Brute Average Approximation Approach for three cases

5.3. Discussion/Conclusion

It was seen that the Rectangle metal fills which is most widely designed when misaligned shows a bigger variation in the epsilon values extracted from the Oblique Incidence Method (i.e variation of 22.5% for the permittivity and 8% for the permeability) as the mutual capacitance increases between layers. So, to reduce the impact of epsilon variations, two approaches are used. First, the rectangle metal fills were aligned and we immediately see that the epsilon variation difference drops down to 9.3% for the permittivity and permeability around 4%. Next, by designing optimal metal fill shapes (i.e. Plus and Hexagon Donut), we see a further reduction in the epsilon variation. For the Plus Aligned metal fill, the permittivity variation is about 6.5% and permeability variation is 3.84%. This was followed by the Hexagon Donut Aligned metal fill where the permittivity variation was close to 7.8% and the permeability variation is about 4%. The aim of this is to see that for less epsilon variations, we can make a better approximation for the scalar number in order to enable to 2.5D EM simulations with less error and therefore the validation of the Design Based Approach for the scalar number extraction is performed for the CPWG structure. This scalar number is extracted using the i) Electric Field Approach and ii) Brute Average Approximation Approach. The metal fill shapes have been categorized into three cases based on the impact of epsilon variations i.e i) Worst Case : Rectangle Misaligned metal fill, ii) Intermediate Case : Rectangle Aligned metal fill, iii) Best Case: Plus Aligned metal fill. By applying the WCB error metric for the two scalar number approaches by having the Oblique Incidence Method as a reference case, we see the least error value for the Electric Field Approach extracted for the Best Case: Plus Aligned metal fill and highest error for the Brute Average Approximation Approach for the Worst Case : Rectangle Misaligned metal fill and from this we can understand that the Electric Field Approach will work perfectly for Transmission line structures as extracting the field can be done easily and hence the percentage of error is less. But for structures like Transformers and Inductors, extracting the field is really complicated and hence it is good to arrive at a solution that has metal fills with less epsilon variation and therefore even use the Brute Average Approximation Approach where the percentage of error is less.

6. Conclusion And Future Scope

6.1. Summary And Conclusion

6.1.1. Summary

It is important to understand that the metal fills do have an impact on the performance of the structures and the impact becomes stronger as the frequency increases due to the parasitics. The impact of the parasitics given by the fabrication process and design rule regulations becomes more predominant as the frequency increases. It is not feasible to directly include the metal fills in the design flow due to drastic increase in the simulation time. The Quasistatic Based Approach that takes into account simple formulations is not suitable for modern commercial EM tools which does not account for the edge effects and hence extracting equivalent permittivity values was difficult and therefore requires periodic boundary conditions to be applied so that the edge effect becomes negligible. This simulation needs to be repeated in three axes to extract the diagonal permittivity behavior and the permeability extraction would require a structure with a series current flowing to compute the magnetic field and extract the inductance parameter and therefore the permeability of the structure requiring multiple simulations. Therefore, the Oblique Incidence Based Method is used which takes into account a single structure that provides the same set of information based on the reflection coefficient provided by TE and TM excitation under two angle of incidence (i.e. normal and oblique) and this would limit the number of simulations to be run and hence makes the approach more efficient for embedding in the design flow. Then the Design Flow Methodology is proposed. Next, by making use of the Oblique Incidence Method, two Scalar Number Approaches are proposed namely Electric Field Approach and Brute Average Approximation Approach that enables the extraction of a scalar number for the permittivity and permeability with improved accuracy for the 2.5D EM solvers from a 3D EM solver. Finally, Design Based Approach for different metal fill shapes and alignment was studied by making use of the Oblique Incidence Method. This is done in order to understand the variations in epsilon effective parameters because for less epsilon variations, an accurate scalar number value can be extracted using the two approaches (i.e. Electric Field Approach and Brute Average Approximation Approach) to enable 2.5D EM simulations with improved accuracy.

6.1.2. Conclusion

In **Chapter 2**, analysis of extracting the epsilon values was done using the Quasistatic Approach by making use of simple mathematical approximation for the parallel plate capacitor case. To extract μ and ε for a bi-anisotropic (i.e. extracting permittivity and permeability) it was seen that multiple simulations using different reference structures (i.e. capacitor and metal strip) needs to be employed under different excitations and hence makes this approach less direct in it's implementation in an automated design flow to support integrated circuit designs. For this reason, it was seen in the literature that the Oblique Incidence Method makes use of the S Parameters that are derived from the normal and oblique incidence for the vertical (TE) and horizontal (TM) components. This is done in order to extract the effective parameters to take into account the effect of metal fills by making use of a single structure. Hence, it makes the approach to be more systematic and efficient for embedding in the design flow for integrated circuit designs. Apart from this, it also has the added advantage of reduced simulation time and good accuracy.

Chapter 3 provided the knowledge about the Unit Cell Approach to extract the epsilon effective parameters for periodic planar structures (i.e. metal fills) using the Oblique Incidence Method and this approach was validated for three cases which are i) Homogeneous material case- which is uniform in all directions, ii) Anisotropic material case - which is direction dependent and iii) Metal Fill Inclusion case - this is done by having the ADL Tool developed by Terahertz Sensing group as a reference which takes into account zero thickness for the metal fills. Furthermore, an explanation of the entire design flow methodology starting from the design in 2.5D EM tool to the 3D EM Tool by making use of the GDS files, Technology files and LayerMap files and then incorporating the Oblique Incidence Method to the structures is given. The advantage of using this design flow methodology is that the effect of metal fills can be directly embedded in the usual design flow process before it goes out to the DRC check stage and therefore to the fabrication stage. The usage of the equivalent layer can be done quite accurately using 3D EM solvers where permittivity and permeability tensor can be employed and is less accurate in 2.5D EM solver where only a scalar number can be provided. As a consequence of this, two Scalar Number Approaches namely Electric Field Approach and Brute Average Approximation Approach were discussed which makes use of the Oblique Incidence Method and therefore this scalar number can enable 2.5D EM simulations with better accuracy.

In **Chapter 4**, validation of the Oblique Incidence Method for the 3D EM tool was done for two test cases which are wave propagating structure (i.e. CPWG with bottom layer metal fills (M2-M6)) and lumped structure (i.e. Stacked Transformer with top layer metal fills (M7-M8)) which was provided by NXP Semiconductors. The advantage of using a CPWG structure is that it providest provides good field confinement in the dielectric below the line and gives low loss performance. The WCB error metric is used for the S Parameters to compare the performances of the CPWG structure for two cases i) removing the metal fills by having the same dielectric

values (i.e. nominal layer values) and ii) using the Oblique Incidence Method by having the metal fill case as the reference to have an understanding of the impact of the metal fills. A lower error value was seen for the case with the Oblique Incidence Method when compared to the case with no metal fills using the nominal layer stack values. However, if we have to simulate the CPWG structure with all the metal fills, the simulation time drastically increases. Therefore, the use of the Oblique Incidence Method which takes into account the effect of metal fills as complex effective parameter values gives the result with good accuracy and reduced simulation time. Moving to the Stacked Transformer case, we observe that it provides the advantage of giving recommended coupling factors with low area-budget and it is also fully-compatible with standard IC process technology. The critical parameters like the Inductance of the Primary (Ls) and Secondary coil of the Transformer(Lp), Mutual Inductance (MI), Quality Factor (Q), Coupling Coefficient (K) and Power Gain of the Transformer (PG) is analysed to compare the performances of the Stacked Transformer structure for three cases i) all the metal fills present in the Stacked Transformer is considered as the reference, ii) removing the metal fills by having the nominal layer values , iii) using the oblique incidence method at three different frequencies (5GHz, 20GHz and 40GHz) to take into account the effect of metal fills as complex effective parameters. Similar to the CPWG structure, the case without metal fill using the nominal layer stack values showed fair amount deviation with frequency when compared to the metal fill case (reference). Therefore, it is important to consider the Oblique Incidence Method which takes into account the effect of metal fills with reduced simulation time and shows good accuracy with the metal fill case. It is also important to note that the effect of metal fills at different frequencies overlaps each other and therefore we can understand that this method is frequency independent. Furthermore, validation of the Scalar Number Approaches (Electric Field Approach and Brute Average Approximation Approach) for the 2.5D EM tool which makes use of the Oblique Incidence Method was performed for the CPWG test structure and the WCB error metric was taken into account for i) Oblique Incidence Method, ii) Electric Field Approach, iii)Brute Average Approximation and iv) No Fills having the same nominal layer value by having the metal fill case as the reference. It was seen that the error from the Electric Field Approach was less than that of the Brute Average Approximation Approach due to the presence of field in the horizontal and vertical component and then applying the weighted average to it and this scalar number could enable 2.5D EM simulation for the transmission line structures since the fields for these structures can be extracted easily.

The Design Based Approach using the Oblique Incidence Method was done in **Chapter 5** for different metal fill shapes and alignment. The Rectangle metal fills which is most widely used but when misaligned will have greater epsilon variations because of the increased mutual capacitance between metal layers. For less epsilon variations a better approximation for the scalar number can be taken by using the Electric Field Approach and Brute Average Approximation Approach in order to enable 2.5D EM simulations with less error. In order to reduce the epsilon variation impact, two approaches were used: i) Aligning the Rectangle metal fill shape

where we already see a reduction in epsilon variation and ii) Designing optimal metal fill shapes, where in this thesis work, we have considered Plus and Hexagon Donut, we can further understand that the epsilon variation reduced even more. The Plus Aligned metal fill shape had the least epsilon variation impact. Moreover, validation of this approach for the scalar number extraction is done for CPWG structure by considering three cases based on epsilon variation which is i) Worst Case - Rectangle Misaligned, ii) Intermediate Case - Rectangle Aligned and iii) Best Case - Plus Aligned in order to extract a scalar number using the Electric Field Approach and Brute Mean Approximation Approach. The WCB error metric for the two scalar number approaches is provided by having the Oblique Incidence Method as a reference. The least error value is seen for the Electric Field Approach extracted for the Best Case: Plus Aligned metal fill and highest error is seen for the Brute Average Approximation Approach extracted the Worst Case : Rectangle Misaligned metal fill. This is because the Electric Field Approach takes into account the field information in the vertical and horizontal directions (weighted average) which gives more insight and knowledge for the epsilon values and this can be used for Transmission line structures as extracting the fields at each crossection of the line can be done easily when compared to the lumped structures like the Transformers and Inductors. For the latter mentioned structures, it is good to arrive at a solution that has metal fills with less epsilon variation which in this case is the Plus Aligned metal fills and hence even use the Brute Average Approximation Approach where the percentage of error is less.

6.2. Future Scope

The work done in this thesis has highlighted the importance of including the metal fills. To accommodate the metal fills for high frequency systems, the following are some of the future works that can be conducted as a continuation to this thesis work:

Design Flow Automated Process: In Chapter 3, the Design Flow Methodology has been elucidated. It is a slightly tedious process for the Design Engineers to manually create all the files and follow all the steps in order to extract complex epsilon values. An automated process which can directly take into account the GDS files, setting up boundary conditions, Floquet ports and extracting the S Parameters and placing it in MATLAB script etc, can be looked into by making use of the scripting language provided by the EM tool (for eg: Python script). With this automated process, the errors can be minimized and the time to set up the entire process can also be reduced.

Measurement Data: Within this thesis project, we have performed a set of validations of the Oblique Incidence Method by having a certain metal fill density composition that could be simulated, but for real structures like the Inductors or Transmission lines where there is very high density of metal fill composition, it is not possible to validate with the EM tool due to high simulation time and memory

usage. It was not possible with the given time frame of the thesis project to perform the measurement of structures for the proof of the Oblique Incidence Method and this can be looked into as a next step. The measurements of these test structures should be well organised with the technology of interest (for eg: 28nm).

A. Appendices

A.1. MATLAB CODE - Oblique Incidence Method

```matlab
clc;
clear;
% Real part - 0
T_real_0=table2array(readtable('S Parameter Plot 15.csv'));

% Imaginary part - 0
T1_imag_0=table2array(readtable('S Parameter Plot 16.csv'));

% Real part - 30
T_real_30=table2array(readtable('S Parameter Plot 17.csv'));

% Imaginary part - 30
T1_imag_30=table2array(readtable('S Parameter Plot 18.csv'));


x=[5:15];
% This represents S parameters at theta=0
S11_TE_real_0= T_real_0(x,2);
S11_TE_imag_0= T1_imag_0(x,2);

% Represents S11-TE
S11_TE_0= S11_TE_real_0+1j.*(S11_TE_imag_0);

S21_TE_real_0= T_real_0(x,3);
S21_TE_imag_0= T1_imag_0(x,3);

% Represents S21-TE
S21_TE_0= S21_TE_real_0+1j.*(S21_TE_imag_0);

S11_TM_real_0= T_real_0(x,4);
S11_TM_imag_0= T1_imag_0(x,4);

% Represents S11-TM
S11_TM_0= S11_TM_real_0+1j.*(S11_TM_imag_0);
```

```
35
36  S21_TM_real_0= T_real_0(x,5);
37  S21_TM_imag_0= T1_imag_0(x,5);
38
39  % Represents S21-TM
40  S21_TM_0= S21_TM_real_0+1j.*(S21_TM_imag_0);
41
42  % This represents S parameters at theta=30 (oblique incidence)
43
44  S11_TE_real_30 = T_real_30(x,2);
45  S11_TE_imag_30= T1_imag_30(x,2);
46
47   % Represents S11-TE
48  S11_TE_30= S11_TE_real_30+1j.*(S11_TE_imag_30);
49
50  S21_TE_real_30= T_real_30(x,3);
51  S21_TE_imag_30= T1_imag_30(x,3);
52
53  % Represents S21-TE
54  S21_TE_30= S21_TE_real_30+1j.*(S21_TE_imag_30);
55
56  S11_TM_real_30= T_real_30(x,4);
57  S11_TM_imag_30= T1_imag_30(x,4);
58
59  % Represents S11-TM
60  S11_TM_30= S11_TM_real_30+1j.*(S11_TM_imag_30);
61
62  S21_TM_real_30= T_real_30(x,5);
63  S21_TM_imag_30= T1_imag_30(x,5);
64
65  % Represents S21-TM
66  S21_TM_30= S21_TM_real_30+1j.*(S21_TM_imag_30);
67
68  % Frequency
69
70  freq=T_real_0(x,1).*10^9;
71
72  % Angle (Theta)
73
74  angle_1=0; %Represents Theta=0
75  angle_2=30; %Represents Theta=30
76
77  % Freespace Wavenumber
78
79  k0=2*pi*(freq)./(3*10^8);
```

74

```matlab
80
81
82  % d is thickness (Height of the dielectric)
83
84  d=0.79*10^-6;
85
86  % Branch indices m and m1
87
88  m=0.000000037;
89  m1=0.00000031;
90
91
92  % Wave Impedance TE at normal incidence (theta=0)
93
94  WI_TE_0= sqrt(((1+S11_TE_0).^2-(S21_TE_0).^2)./((1-S11_TE_0)
       .^2-(S21_TE_0).^2)).*sec(angle_1);
95
96  % Wave Impedance TE at oblique incidence (theta=30)
97
98  WI_TE_30= sqrt(((1+S11_TE_30).^2-(S21_TE_30).^2)./((1-
       S11_TE_30).^2-(S21_TE_30).^2)).*sec(angle_2*pi/180);
99
100 % Wave Impedance TM at normal incidence (theta=0)
101
102 WI_TM_0= sqrt(((1+S11_TM_0).^2-(S21_TM_0).^2)./((1-S11_TM_0)
       .^2-(S21_TM_0).^2)).*cos(angle_1);
103
104 % Wave Impedance TM at oblique incidence (theta=30)
105
106 WI_TM_30= sqrt(((1+S11_TM_30).^2-(S21_TM_30).^2)./((1-
       S11_TM_30).^2-(S21_TM_30).^2)).*cos(angle_2*pi/180);
107
108
109 % Sigma TE at normal incidence (theta=0)
110
111   e=1-(S11_TE_0.*(WI_TE_0.*cos(angle_1)-1))./(WI_TE_0.*cos(
       angle_1)+1); %Represents the denominator
112
113   Sigma_TE_0= S21_TE_0./e;
114
115 % Sigma TE at oblique incidence (theta=30)
116
117   p=1-(S11_TE_30.*(WI_TE_30.*cos(angle_2*pi/180)-1))./(WI_TE_30
       .*cos(angle_2*pi/180)+1); %Represents the denominator
118
```

```matlab
119    Sigma_TE_30= S21_TE_30./p;
120
121  % Sigma TM at normal incidence (theta=0)
122
123    r=1-(S11_TM_0.*((WI_TM_0./cos(angle_1))-1))./(WI_TM_0./cos(
         angle_1)+1); %Represents the denominator
124
125    Sigma_TM_0= S21_TM_0./r;
126
127     % Sigma TM at oblique incidence (theta=30)
128
129    w=1-(S11_TM_30.*((WI_TM_30./cos(angle_2*pi/180))-1))./(
         WI_TM_30./cos(angle_2*pi/180)+1); %Represents the
         denominator
130
131    Sigma_TM_30= S21_TM_30./w;
132
133
134  % Refractive index TE at normal incidence (theta=0)
135
136  RI_TE_0= sqrt(((log(abs(Sigma_TE_0))+1j.*(angle(Sigma_TE_0)+2*
         pi*m))./(-1j.*k0.*d)).^2+sin(angle_1).^2);
137
138  % Refractive index TE at oblique incidence (theta=30)
139
140  RI_TE_30= sqrt(((log(abs(Sigma_TE_30))+1j.*(angle(Sigma_TE_30)
         +2*pi*m))./(-1j.*k0.*d)).^2+sin(angle_2*pi/180).^2);
141
142  % Refractive index TM at normal incidence (theta=0)
143
144  RI_TM_0= sqrt(((log(abs(Sigma_TM_0))+1j.*(angle(Sigma_TM_0)+2*
         pi*m1))./(-1j.*k0.*d)).^2+sin(angle_1).^2);
145
146  % Refractive index TM at oblique incidence (theta=30)
147
148  RI_TM_30= sqrt(((log(abs(Sigma_TM_30))+1j.*(angle(Sigma_TM_30)
         +2*pi*m1))./(-1j.*k0.*d)).^2+sin(angle_2*pi/180).^2);
149
150
151  % Epsilon Permittivity - Ex
152
153  Ex=(RI_TM_0)./(WI_TM_0);
154
155  % Epsilon Permittivity - Ey
156
```

```matlab
157  Ey=(RI_TE_0)./(WI_TE_0);
158
159  % Epsilon Permittivity 1 - Ez 1
160
161  Ez_1=Ex.*sin(angle_2*pi/180).^2./(sin(angle_2*pi/180).^2-(
         RI_TM_30).^2+(RI_TM_0).^2);
162
163  % Epsilon Permittivity 2 - Ez 2
164
165  Ez_2=sin(angle_2*pi/180).^2./((RI_TM_0.*WI_TM_0)-Ex.*(WI_TM_30
         ).^2);
166
167  % Epsilon Permeability - Mx
168
169  Mx=(RI_TE_0).*(WI_TE_0);
170
171  % Epsilon Permeability - My
172
173  My=(RI_TM_0).*(WI_TM_0);
174
175  % Epsilon Permeability 1 - Mz 1
176
177  Mz_1=sin(angle_2*pi/180).^2./((RI_TE_0./WI_TE_0)-Mx./(WI_TE_30
         ).^2);
178
179  % Epsilon Permeability 1 - Mz 2
180
181  Mz_2=Mx.*sin(angle_2*pi/180).^2./(sin(angle_2*pi/180).^2-(
         RI_TE_30).^2+(RI_TE_0).^2);
```

A.2. MATLAB CODE - Scalar Number Extraction (Field Extraction)

```matlab
clc;
clear;

% Taking Real and Imaginary values

E_real=readtable('real_cpwg_3');
E_imag=readtable('imag_cpwg_3');
H_real=readtable('H_real_cpwg');
H_imag=readtable('H_imag_cpwg');

% Making it a complex number

Ey_complex=table2array(E_real(:,5))+1i*table2array(E_imag(:,5));
Ez_complex=table2array(E_real(:,6))+1i*table2array(E_imag(:,6));
Hy_complex=table2array(H_real(:,5))+1i*table2array(H_imag(:,5));
Hz_complex=table2array(H_real(:,6))+1i*table2array(H_imag(:,6));

% Taking the Magnitude

Ey_Mag=abs(Ey_complex);
Ez_Mag=abs(Ez_complex);
Hy_Mag=abs(Hy_complex);
Hz_Mag=abs(Hz_complex);


% Taking the total intensity

Sum_Ey=sum(Ey_Mag);
Sum_Ez=sum(Ez_Mag);
Sum_Hy=sum(Hy_Mag);
Sum_Hz=sum(Hz_Mag);

% Total intensity

Total_sum=Sum_Ey+Sum_Ez;
Total_sum_1=Sum_Hy+Sum_Hz;

```

```matlab
% Percentage of Ey

Percentage_Ey =(Sum_Ey/Total_sum )*100;
% Percentage of Ez

Percentage_Ez =(Sum_Ez/Total_sum )*100;
% Percentage of Hy

Percentage_Hy =(Sum_Hy/Total_sum_1)*100;
% Percentage of Hz

Percentage_Hz =(Sum_Hz/Total_sum_1)*100;

% Scaling the Permittivity and Permeability value from the
    Field contribution

Ey=4.4111*(Percentage_Ey /100);
Ez=4.116*(Percentage_Ez /100);
My=1.075*(Percentage_Hy /100);
Mz=1.034*(Percentage_Hz /100);

Scalar_Permittivity =Ey+Ez;
Scalar_Permeability =My+Mz;
```

Bibliography

[1] V. S. Shilimkar and A. Weisshaar, "Modeling of metal-fill parasitic capacitance and application to on-chip slow-wave structures," *IEEE Transactions on Microwave Theory and Techniques*, vol. 65, pp. 1456–1464, 2017.

[2] A. Allan, D. Edenfeld, Joyner, A. Kahng, M. Rodgers, and Y. Zorian, "2001 technology roadmap for semiconductors," *Computer*, vol. 35, pp. 42–53, 02 2002.

[3] J.-A. Carballo, W.-T. J. Chan, P. A. Gargini, A. B. Kahng, and S. Nath, "Itrs 2.0: Toward a re-framing of the semiconductor technology roadmap," in *2014 IEEE 32nd International Conference on Computer Design (ICCD)*, 2014, pp. 139–146.

[4] Wikipedia, "Semiconductor device fabrication — Wikipedia, the free encyclopedia," http://en.wikipedia.org/w/index.php?title=Semiconductor%20device%20fabrication&oldid=1104211175, 2022, [Online; accessed 03-September-2022].

[5] "International Technology Roadmap for Semiconductors," http://www.itrs2.net/, 2022, [Online; accessed 03-September-2022].

[6] A. Islam, "Technology scaling and its side effects," in *2015 19th International Symposium on VLSI Design and Test*, 2015, pp. 1–1.

[7] S. Borkar, "Design challenges of technology scaling," *IEEE Micro*, vol. 19, no. 4, pp. 23–29, 1999.

[8] R. Tian, D. Wong, and R. Boone, "Model-based dummy feature placement for oxide chemical-mechanical polishing manufacturability," *IEEE Transactions on Computer-Aided Design of Integrated Circuits and Systems*, vol. 20, no. 7, pp. 902–910, 2001.

[9] A. B. Kahng and R. O. Topaloglu, "A doe set for normalization-based extraction of fill impact on capacitances," in *8th International Symposium on Quality Electronic Design (ISQED'07)*, 2007, pp. 467–474.

[10] J. Kim, S. Ahn, K. Choe, A. Saleh, and M. Alimam, "A novel framework for checking and automating drc rules," in *2022 IEEE 31st Microelectronics Design Test Symposium (MDTS)*, 2022, pp. 1–3.

[11] "Synopsys — EDA Tools, Semiconductor IP and Application Security Solutions — synopsys.com," https://www.synopsys.com/, [Accessed 03-Sep-2022].

[12] "Design for manufacturability and new layout rules," https://web.stanford.edu/, [Accessed 03-Sep-2022].

[13] J. Carroll and J. Dunn, "Electromagnetic simulation challenges in rfic design," 01 2016, pp. 81–83.

[14] P. Monk, *Finite Element Methods for Maxwell's Equations (Numerical Analysis and Scientific Computation Series)*, 01 2003.

[15] D. K. Sun, Z. Cendes, and J.-F. Lee, "Adaptive mesh refinement, h-version, for solving multiport microwave devices in three dimensions," *IEEE Transactions on Magnetics*, vol. 36, no. 4, pp. 1596–1599, 2000.

[16] K.-J. Chang, J.-J. Chou, H.-C. Li, and K.-C. Chang, "Impact quantification of the dummy metal fills on nanometer vlsi designs for dfm," in *2008 IEEE International Symposium on VLSI Design, Automation and Test (VLSI-DAT)*, 2008, pp. 291–294.

[17] A. Kuriakose, "Parallel plate capacitors and their properties," 09 2020.

[18] S. Grimnes and Martinsen, *Bioimpedance and Bioelectricity Basics: Third Edition*, 01 2014.

[19] D. Smith, S. Schultz, P. Markoš, and C. Soukoulis, "Determination of negative permittivity and permeability of metamaterials from reflection and transmission coefficients," *Physical Review B*, vol. 65, 11 2001.

[20] X. Chen, T. Grzegorczyk, B.-I. Wu, J. Pacheco, and J. Kong, "Robust method to retrieve the constitutive effective parameters of metamaterials," *Physical review. E, Statistical, nonlinear, and soft matter physics*, vol. 70, p. 016608, 02 2004.

[21] D. Smith, D. Vier, T. Koschny, and C. Soukoulis, "Electromagnetic parameter retrieval from inhomogeneous metamaterials," *Physical review. E, Statistical, nonlinear, and soft matter physics*, vol. 71, p. 036617, 04 2005.

[22] Z. Li, K. Aydin, and E. Ozbay, "Determination of the effective constitutive parameters of bianisotropic metamaterials from reflection and transmission coefficients," *Physical review. E, Statistical, nonlinear, and soft matter physics*, vol. 79, p. 026610, 03 2009.

[23] D. Zarifi, M. Soleimani, and A. Abdolali, "Electromagnetic characterization of biaxial bianisotropic media using the state space approach," *Antennas and Propagation, IEEE Transactions on*, vol. 62, pp. 1538–1542, 03 2014.

[24] M. Smierzchalski and K. Mahdjoubi, "A novel approach for the characterization of bi-anisotropic metamaterials using oblique incidence," in *2013 7th International Congress on Advanced Electromagnetic Materials in Microwaves and Optics*, 2013, pp. 511–513.

[25] D. Cohen and R. Shavit, "Bi-anisotropic metamaterials effective constitutive parameters extraction using oblique incidence s-parameters method," *IEEE Transactions on Antennas and Propagation*, vol. 63, no. 5, pp. 2071–2078, 2015.

[26] D. Cavallo and C. Felita, "Analytical formulas for artificial dielectrics with non-aligned layers," *IEEE Transactions on Antennas and Propagation*, vol. 65, no. 10, pp. 5303–5311, 2017.

[27] "ANSYS HFSS — Ansys Innovation Couses," https://courses.ansys.com/index.php/courses/ansys-hfss-floquet-port/, 2022, [Online; accessed 03-September-2022].

[28] A. B. Numan and M. S. Sharawi, "Extraction of material parameters for metamaterials using a full-wave simulator [education column]," *IEEE Antennas and Propagation Magazine*, vol. 55, no. 5, pp. 202–211, 2013.

[29] P. Kovacs and Z. Raida, "Dispersion analysis of planar metallo-dielectric ebg structures in ansoft hfss," in *MIKON 2008 - 17th International Conference on Microwaves, Radar and Wireless Communications*, 2008, pp. 1–4.

[30] E. Klumperink, R. Kreienkamp, T. Ellermeyer, and U. Langmann, "Transmission lines in cmos: An explorative study," *Requirements Engineering - RE*, 01 2001.

[31] M.-J. Nie, X.-X. Yang, G.-N. Tan, and B. Han, "A compact 2.45-ghz broadband rectenna using grounded coplanar waveguide," *IEEE Antennas and Wireless Propagation Letters*, vol. 14, pp. 986–989, 2015.

[32] J. Yunas, A. Hamzah, and B. Majlis, "Surface micromachined on-chip transformer fabricated on glass substrate," *Microsystem Technologies*, vol. 15, pp. 547–552, 04 2009.

[33] E. Klumperink, R. Kreienkamp, T. Ellermeyer, and U. Langmann, "Transmission lines in cmos: An explorative study," *Requirements Engineering - RE*, 01 2001.

[34] D. F. Williams and R. B. Marks, "Calibrating on-wafer probes to the probe tips," in *40th ARFTG Conference Digest*, vol. 22, 1992, pp. 136–143.

[35] D. Cavallo and R. M. van Schelven, "Closed-form analysis of artificial dielectric layers with non-periodic characteristics," in *2019 13th European Conference on Antennas and Propagation (EuCAP)*, 2019, pp. 1–5.

[36] M. Nelson, "Optimized pattern fill process for improved cmp uniformity and interconnect capacitance," in *Proceedings of the 15th Biennial University/Government/ Industry Microelectronics Symposium (Cat. No.03CH37488)*, 2003, pp. 374–375.